esearch Laboratory
: 20375-5000

NRL Report 9244

Sea Clutter

L. B. WETZEL

Senior Scientist and Propagation Staff
Radar Division

September 28, 1990

CONTENTS

SEA CLUTTER

INTRODUCTION

For an operational radar, backscatter of the transmitted signal by elements of the sea surface often places severe limits on the detectability of returns from ships, aircraft, missiles, navigation buoys, and other targets sharing the radar resolution cell with the sea. These interfering signals are commonly referred to as *sea clutter*, or *sea echo*. Since the sea presents a dynamic, endlessly variable face to the radar, an understanding of sea clutter depends not only on finding suitable models to describe the surface scattering but also on knowledge of the complex behavior of the sea. Fortunately, a close relationship between radar and oceanography has grown up in the remote sensing community. This relationship has provided a large amount of useful information about scattering from the sea and how this scattering relates to oceanographic variables.

Characterizing sea clutter empirically by direct measurement of radar returns for a wide variety of both the radar and environmental parameters would appear to be simple. Parameters relating to the radar or its operating configuration—such as frequency, polarization, cell size, and grazing angle—can be specified by the experimenter. However, the environmental parameters are quite another matter—for two reasons. First, it has not always been clear which environmental variables are important. For example, wind speed certainly seems to affect clutter levels, but correlation of clutter with, say, ships' anemometer readings has not been entirely satisfactory. The state of agitation of the surface (*sea state*) appears to have a strong effect, but it is a subjective measure, and its relation to the prevailing local winds is often uncertain. Moreover, temperatures of the air and the sea surface can affect the way in which the measured wind speed is related to the generation of clutter-producing waves. The importance of these effects, however, were unappreciated over most of the history of sea clutter measurements, so air and sea temperatures were seldom recorded. Even if the importance of an environmental parameter has been recognized, it is often difficult to measure it with accuracy under real-sea conditions. There are practical and budgetary limits to obtaining open ocean measurements in sufficient variety to develop any really meaningful statistical models of clutter. Little wonder that many aspects of sea clutter remain frustratingly ill-defined.

Before the late 1960s, most clutter data were collected in bits and pieces from isolated experiments, often with poor, or incomplete, ground truth. (For reviews of the older literature, see, for example, Long [1], Skolnik [2], or Nathanson [3]). Nevertheless, although much of the earlier clutter data were of limited scientific value, they did show some general trends, such as the tendency of clutter signal strength to increase with the grazing angle and wind speed (or *sea state*) at low to intermediate grazing angles, and generally to be greater for vertical polarization and in upwind/downwind directions.

The appearance of sea clutter when viewed on an A-scope depends strongly on the size of the resolution cell, or *radar footprint*. For large cells it appears "distributed" in range and can be characterized by a surface-averaged cross section with relatively modest fluctuations about a mean

Manuscript approved October 12, 1989.

value. As the size of the resolution cell is reduced, clutter takes on the appearance of isolated target-like, or *discrete*, returns that vary in time. At these higher resolutions, the *distributed* clutter is often seen to consist of a dense sequence of discrete returns. When the discrete returns stand well out of the background, as they are seen to do for both polarizations (but most clearly with horizontal polarization at small grazing angles), they are called *sea spikes* and are a common clutter contaminant in this radar operating regime.

Attempts to provide a theoretical explanation of the observed behavior of clutter signals trace essentially from the early work pursued during World War II. These efforts are described in the well-known MIT Radiation-laboratory book edited by Kerr [4]. Unfortunately, the scattering models developed during this period, and most of those published over the following decade, failed to account for the behavior of sea backscatter in a very convincing way. In 1956, however, Crombie [5] observed that at high frequency (HF) wavelengths (tens of meters) scattering appeared to arise from a resonant interaction with sea waves of one half the incident wavelength, i.e., to be of the Bragg type. Reinforced by the theoretical implications of various small waveheight approximations and wavetank measurements under idealized conditions, the *Bragg model* was introduced into the microwave regime by researchers in the mid-1960s [6-8]. This produced a revolution in thinking about the origins of sea clutter because it involved the sea wave spectrum, thus forging a link between clutter physics and oceanography in what became the field of *radio oceanography*. However, fundamental conceptual problems in applying the Bragg hypothesis in microwave scattering, with recent questions about the validity of its predictions and the possibility of alternative scattering hypotheses, have reopened inquiry into the physical origins of sea scatter and how best to model it [9-14]. This being the case, in this report speculation about physical models is kept to a minimum in the sections on the empirical behavior of sea clutter. The problem of modeling sea scatter is discussed separately in a later section.

DESCRIPTION OF THE SEA SURFACE

Close observation of the sea surface discloses a variety of features such as wedges, cusps, waves, foam, turbulence, and spray, as well as breaking events of all sizes and masses of falling water. Any, or all, of these might contribute to the scattering of electromagnetic waves responsible for sea clutter. The basic oceanographic descriptor of the sea surface, however, is the *wave spectrum*, which, while saying little about individual features, contains a great deal of information about the sea surface in general. It is also central to the application of the Bragg scattering hypothesis. Because of the need to understand the sea surface in order to understand sea clutter and the prominence of the Bragg hypothesis in existing clutter models, some tutorial material describing the spectral characterization of the sea surface is included below.

Basically there are two types of surface waves—capillary and gravity—depending on whether surface tension or gravity is the dominant restoring force. The transition between one and the other takes place at a wavelength of ~ 2 cm. Thus the smaller capillary waves supply the surface fine structure, while gravity waves make up the larger and most visible surface structures. Waves have their origin ultimately in the wind, but this does not mean that the *local* wind is a particularly good indicator of what the wave structure beneath it will be. To arouse the surface to its fully developed, or equilibrium state, the wind must blow for a sufficient time (Duration) over a sufficient distance (Fetch). That part of the wave structure directly produced by these winds is called Sea. But waves propagate; even in the absence of local wind, significant local wave motion can exist that is the result of waves arriving from far away, perhaps from a distant storm. Waves of this type are called Swell. Because the surface over which the waves travel acts as a low-pass filter, Swell components often take the form of long-crested low-frequency sinusoids.

THE WAVE SPECTRUM

The wave spectrum, which provides the primary oceanographic description of the sea surface, appears in several forms. If the time history of the surface elevation is monitored at a fixed point, the resulting time series may be processed to provide a *frequency spectrum S(f)* of the surface elevation, where $S(f)df$ is a measure of the *energy* (i.e., square of the wave height) in the frequency interval between f and $f + df$. Wave spectra have been measured in the open ocean primarily for gravity waves down to wavelengths of ~ 1 m. Open-ocean measurements of capillary waves are especially difficult to perform [12].

For a gravity wave, the frequency f and wavenumber K are related by the dispersion relation

$$f = (1/2\pi)\,(gK)^{1/2}\,, \tag{1}$$

where g is the acceleration of gravity and $K = 2\pi/\Lambda$, with Λ being the wavelength. Although each individual gravity wave obeys this relation, the waves at a point on the sea surface could come from any direction, so they are characterized by a two-dimensional propagation vector with orthogonal components K_x and K_y, where the K used in Eq. (1) is the magnitude $K = K_x^2 + K_y^2)^{1/2}$.

The wavenumber spectrum associated with $S(f)$ is a function of the two components of K and is commonly written as $W(K_x,K_y)$. This is called the *directional wave spectrum* and expresses the asymmetries associated with conditions such as winds, currents, refraction, and isolated swell components. For a given source of asymmetry, like the wind, various parts of the spectrum display different directional behaviors. For example, in a fully developed sea the larger waves tend to move in the direction of the wind, and the smaller waves are more isotropic. Directional spectra are more difficult to measure and are obtained by a variety of experimental methods. These methods include an array of wave staffs to measure surface heights over a matrix of points, a multiaxis accelerometer buoy, stereo photography, and even processed radar backscatter signals. However, a frequency spectrum measured at a point can contain no knowledge of wave direction, so a wavenumber spectrum $W(K)$ is often defined in terms of the frequency spectrum $S(f)$ by the relation

$$W(K) = S(f\,(K))(df\,/dK)\,. \tag{2}$$

The relation between f and K is as given by Eq. (1). To account for the wind direction, $W(K)$ is sometimes multiplied by an empirical function of K and direction θ relative to the (up)wind direction.

Oceanographers have not always agreed about the form of the frequency spectrum. Nonequilibrium wave conditions, inadequate sampling times, poor ground truth, and other factors can contaminate the data set from which empirical spectra are derived. However, by careful selection of data from many sources, ensuring that only equilibrium (fully developed) sea conditions were represented and the wind was always measured at the same reference height, Pierson and Moskowitz [16] established an empirical spectrum that has proved popular and useful. It has the form

$$s(f) = Af^{-5}e^{-B(f_m/f)^4} \tag{3}$$

where g is the acceleration of gravity, and $f_m = g\,/2\pi\,U$, which corresponds to the frequency of a wave moving with a velocity equal to the wind speed U; A and B are empirical constants. Figure 1 shows this spectrum for several wind speeds. The effect of increasing wind speed is simply to move

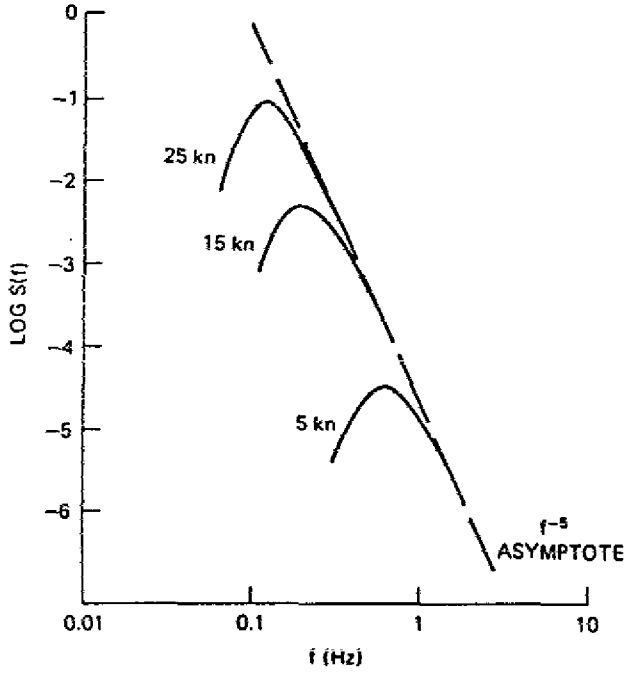

Fig. 1 — Sea wave frequency spectra of the Pierson-Moskowitz type, representing fully developed seas.

the low-frequency *cut-off* to lower frequencies along the high-frequency f^{-5} asymptote. (Most of the oceanographers' spectra are based on measurements at relatively low frequencies; they cannot be taken seriously at frequencies $\gtrsim 2$ Hz. Nevertheless, these spectral forms are often used up to 20 Hz or greater for predicting radar clutter under the Bragg hypothesis.)

Converting this frequency spectrum into an isotropic wavenumber spectrum by using Eq. (2) results in a spectrum of similar form, only with a K^{-4} asymptote. Phillips [17] derived this asymptotic behavior on dimensional grounds. A widely used simplification, obtained by replacing the smooth peak in Fig. 1 by a sharp cut-off, is generally referred to as the *Phillips Spectrum*. In wavenumber space this is written as

$$W(K) = 0.005/K^{-4} \qquad K > g/U^2$$

$$= 0, \qquad K < g/U^2 \tag{4}$$

where the cut-off wavenumber corresponds to the frequency f_m of the peak in Eq. (3). Opposed to this highly simplified form, increasingly complex spectra exist that are based on more careful empirical studies [18] as well as on more sophisticated theoretical considerations [19, 20].

In discussing the characterization of the sea surface by its spectrum, remember that the spectrum is a highly averaged description of how the energy of the surface is distributed among the wavenumbers, or frequencies, of the waves present on it. Since the phases of these waves are lost, the spectrum gives no information about the morphology of the surface itself, i.e., about the complex surface features that are responsible for the scattered field. This point is raised again in the section on theories of sea clutter.

General Sea Descriptors

The shape of the curves in Fig. 1 suggests that the sea wave system has a relatively high Q. Therefore it should be possible to get a rough idea of the behavior of the major waves on the surface by taking the values of *period* $(1/f)$ and *wavelength* $(2\pi/K)$ defined at the spectral peak. These values belong to a wave satisfying the dispersion relation Eq. (1) and having a phase velocity $C = 2\pi f/K$ equal to the wind speed U. By using Eq. (1), the period T and wavelength Λ thereby defined take the form

$$T = 0.64*U; \quad \Lambda = 0.64*U^2 \quad (U \text{ in m/s}). \tag{5}$$

Thus, for example, the largest waves in a fully developed sea for a 15 knot (7.5 m/s) wind will have a wavelength of ~120 ft (36 m) and a period of 5 s.

The statistical distribution of wave heights on the ocean surface is quite close to gaussian, with a mean-square deviation that can be obtained by integrating the wave height spectrum over all frequencies (or wavenumbers). For spectra resembling those in Fig. 1, the rms wave height is given approximately by

$$h_{rms} = 0.005*U^2 \text{ m}. \tag{6}$$

The rms wave height contains contributions from all of the waves on the surface, but often the peak-to-trough height for the higher waves is of major interest. This is certainly the case for a ship in a seaway or in the shadowing of the surface at low radar grazing angles. The *significant height*, or *height of the 1/3 highest waves*, provides such a measure. It is denoted by $H_{1/3}$ and is taken to be about three times the rms height given by Eq. (6). For a 15-knot wind, this is only ~3 ft, but for gale-force winds of 40 knots, it rises to >20 ft, which is a rather formidable sea.

Looking at the sea, an observer might describe what he or she sees in terms of a subjective *state of the sea*, e.g., *smooth*, *rough*, or *terrifying!* If these descriptions are listed in order of severity and assigned numbers, these numbers define a *sea state*. A similar numerical scale exists for wind speeds, the *Beaufort Wind Scale*, with numbers that are an integer or so higher than the corresponding *sea state*. But it is seldom used in reference to sea clutter.

Two numbers, then, are commonly used to indicate the activity of the sea surface: a subjective *sea state* and a measured wind speed. Only when the wind has sufficient fetch and duration to excite a fully developed sea can a wave height be unambiguously associated with it. Table 1 lists the surface descriptors that are generally used in connection with sea clutter—sea state, wind speed, and its associated equilibrium wave height—together with the wind speed in knots, the significant wave height in feet, and the duration/fetch required for a fully developed sea in hours per nautical mile. Note that the median wind speed over the world's oceans is ~15 knots, which corresponds to sea state 3.

EMPIRICAL BEHAVIOR OF SEA CLUTTER

Sea clutter is a function of many parameters, some of which show a complicated interdependence. It is not easy to establish its detailed behavior with a great deal of confidence or precision. For example, in a proper sea clutter measurement, the polarization, radar frequency, grazing angle,

Table 1 — Sea Surface Descriptors

Sea State	Wind Speed (kn)	Wave Height $H^{1/3}$ (ft)	Duration/Fetch (h/nmi)
1 (Smooth)	< 7	< 1	1/20
2 (Slight)	7 - 12	1 - 3	5/50
3 (Moderate)	12 - 16	3 - 5	15/100
4 (Rough)	16 - 19	5 - 8	23/150
5 (Very Rough)	19 - 23	8 - 12	25/200
6 (High)	23 - 30	12 - 20	27/300
7 (Very High)	30 - 45	20 - 40	30/500

and resolution cell size are specified. Then the wind speed and direction must be measured at a reference altitude. If the results are to be compared with those of other experimenters, the proper duration and fetch must be present to ensure standardization to equilibrium sea conditions. Because these measured winds are related to the wind structure at the surface through the atmospheric boundary layer, the shape of this layer must be determined by measuring the air and sea temperatures. To complicate the picture still further, it is becoming increasingly clear that sea backscatter has a strong dependence on the direction of the long waves, which include swell, in the measurement area, so ideally the directional wave spectrum should be measured as well. Obviously, it is unlikely that all of these environmental parameters will be recorded with precision in every (or even any) sea clutter measurement; considerable variability in the basic conditions under which sea clutter data are collected by different experimenters can be expected.

It is of interest to note that in many of the reported measurements of sea clutter, particularly in the older literature, wide inconsistencies between wind speed and wave height are found. For example, a wind speed of 5 kn might be reported with wave heights of 6 ft, or 20 kn winds with 2-ft waves. These pairings are inconsistent with the values for an equilibrium sea described in Table 1 and indicate the unnoticed presence of heavy swell or highly nonequilibrium wind conditions, or both. Even with all of the variables properly specified, recorded clutter data can be spread over a wide dynamic range, often as great as 40 dB at low grazing angles, so clutter behavior is best described in terms of probability distribution functions.

Since sea clutter is generally viewed as a surface-distributed process, the basic clutter parameter is taken to be the normalized radar cross section (NRCS) σ^0 of the surface. This is commonly referred to as sigma zero and is expressed in dB relative to 1 m^2/m^2. It is obtained experimentally by dividing the measured radar cross section of an illuminated patch of the surface by a normalizing area. Therefore, differences in the definition of this area can lead to inconsistencies among various reports of NRCS measurements.

Scattering from any distributed target involves the product of the transmitting and receiving system footprints integrated over the target. These footprints cover exactly the same area for a monostatic radar and depend on the pulse and beam widths, the range, and the grazing angle. If the footprints are assumed to be of the *cookie-cutter* type (constant amplitude falling sharply to zero at the half-power points), the relation between the actual clutter cross section σ^c, as inferred from the received power via the radar equation, and the NRCS σ^0 is given by

$$\sigma^0 = \sigma^c / A_f. \tag{7}$$

For a radar with an antenna beamwidth B and rectangular pulse of length T, viewing the surface at range R and grazing angle θ, the area A_f is either

$$A_f = \pi(BR)^2/4 \sin\theta \tag{8}$$

for beam-limited conditions (e.g., continuous wave (CW) or long-pulse radar at high grazing angles), or,

$$A_f = (cT/2)^*(BR)/\cos\theta \tag{9}$$

for pulsewidth-limited conditions (e.g., short-pulse radar at low grazing angles).

Real radars do not produce cookie-cutter footprints, however, since the antenna beam will have a Bessel or gaussian profile and the pulse might be shaped. For this reason, an effective A must be obtained from a surface integration of the square of the actual amplitude profile of the footprint. This will always result in a smaller value of A than that defined by Eqs. (8) or (9), therefore also in larger values of σ^0 as derived from measured values of σ^c by Eq. (7). Most experimenters use the half-power beamwidth in Eqs. (8) or (9), with an error that is usually only 1 or 2 dB.

Dependence on Wind Speed, Grazing Angle, and Frequency

It was noted earlier that summaries of clutter measurements made before about 1970 may be found in several of the standard reference books on radar [2,3] and radar clutter [1]. Among the programs of this period, the most ambitious was that pursued in the late 1960s at the Naval Research Laboratory [21]. In this program an airborne four-frequency radar (4FR), operating with both horizontal and vertical polarizations at UHF (428 MHz), L-band (1228 MHz), C-band (4455 MHz), and X-band (8910 MHz), made clutter measurements upwind, downwind, and crosswind in winds from 5 to 50 kn for grazing angles between 5° and 90°. The system was calibrated against standard metal spheres, and wind speeds and wave heights were recorded in the measurement areas from instrumented ships.

Typically, samples of σ^0 for a given set of radar and environmental parameters are scattered over a wide range of values. In the NRL experiments they were organized into probability distribution functions of the type shown in Fig. 2. The data, represented by the solid line, are plotted on normal probability paper; Rayleigh and lognormal distributions are shown for comparison (dashed lines). The ordinate is percent of time the abscissa is exceeded, and the abscissa is the value of σ^0 as defined by Eq. (7), with A taken from Eqs. (8) or (9) as appropriate. This particular distribution is representative of clutter from a relatively large radar footprint (pulse length about 0.5 μs) measured at intermediate grazing angles (20° to 70°) for moderate wind speeds ($\sim$15 kn). It is Rayleigh-like but shows a tendency toward lognormal behavior for the larger cross sections. From a detailed statistical analysis of the NRL 4FR data, Valenzuela and Laing [22] concluded that for these data, at least, the distributions of sea clutter cross sections were intermediate between the exponential (which is the power distribution corresponding to Rayleigh-distributed scattered-field amplitudes) and lognormal distributions.

Organizing the data samples into probability distributions makes the median (50%) value a convenient statistical measure of the clutter cross section. But many investigators process their data to provide the mean value. Since the conversion of a median to a mean requires knowledge of the probability distribution function, care must be taken to avoid ambiguity in comparing the measurements

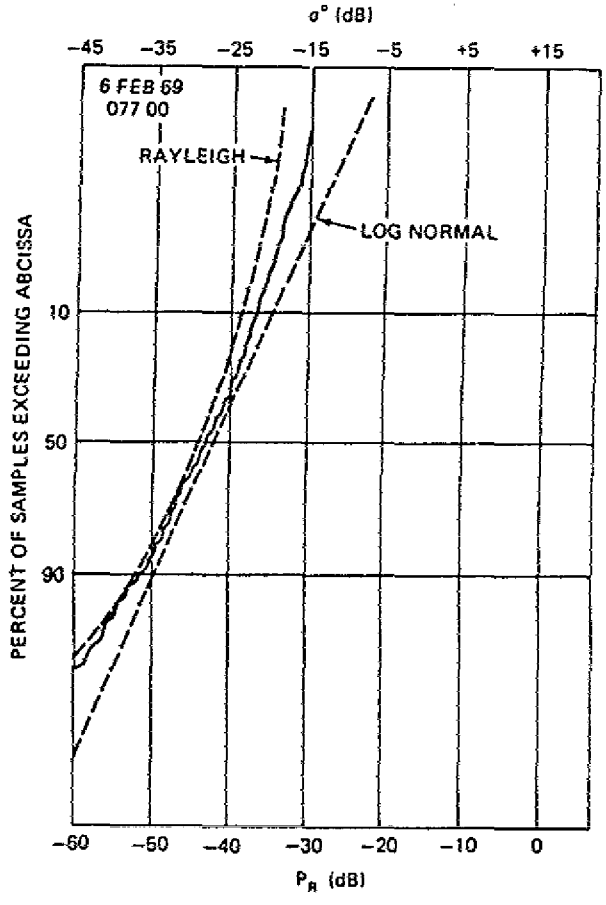

Fig. 2 — An example of the probability distribution of sea clutter data. (From Daley [21].)

of different experimenters. The original analysis of the NRL 4FR data was based on median cross sections and the assumptions of the cookie-cutter antenna beam embodied in Eqs. (8) and (9) [21, 23]. In later presentations of these data [24], the median values of σ^0 were replaced by means, raising them by ~ 1.6 dB, and the area A in Eq. (7) was redefined in terms of a more realistic tapered footprint, adding another 1 to 2 dB. This means that there is a difference of 3 to 4 dB between the earlier and later presentations of the same data. Because these results are widely used and quoted, it is important to ensure that the proper definition of σ^0 is being used when comparing them with clutter data taken by other experimenters or when using them in clutter predictions.

General Results

Because it was the first really comprehensive collection of clutter data over a wide range of radar frequencies, the 4FR program produced many plots showing the dependence of sea clutter on grazing angle, frequency, polarization, wind direction, and wind speed. However, comparing these plots with other plots that were made both earlier and later shows the extent of the variations that are found in sea clutter measurements reported by different investigators for exactly the same set of parameters. This is seen clearly in Fig. 3, which compares the grazing angle dependence of X-band clutter data for ~ 15 kn wind speeds obtained from four sources: NRL-4FR [24] (these are mean results for upwind directions and include the antenna corrections mentioned above); recent aircraft measurements by Masuko et al. [29] (also in the upwind direction); and summaries of the older data

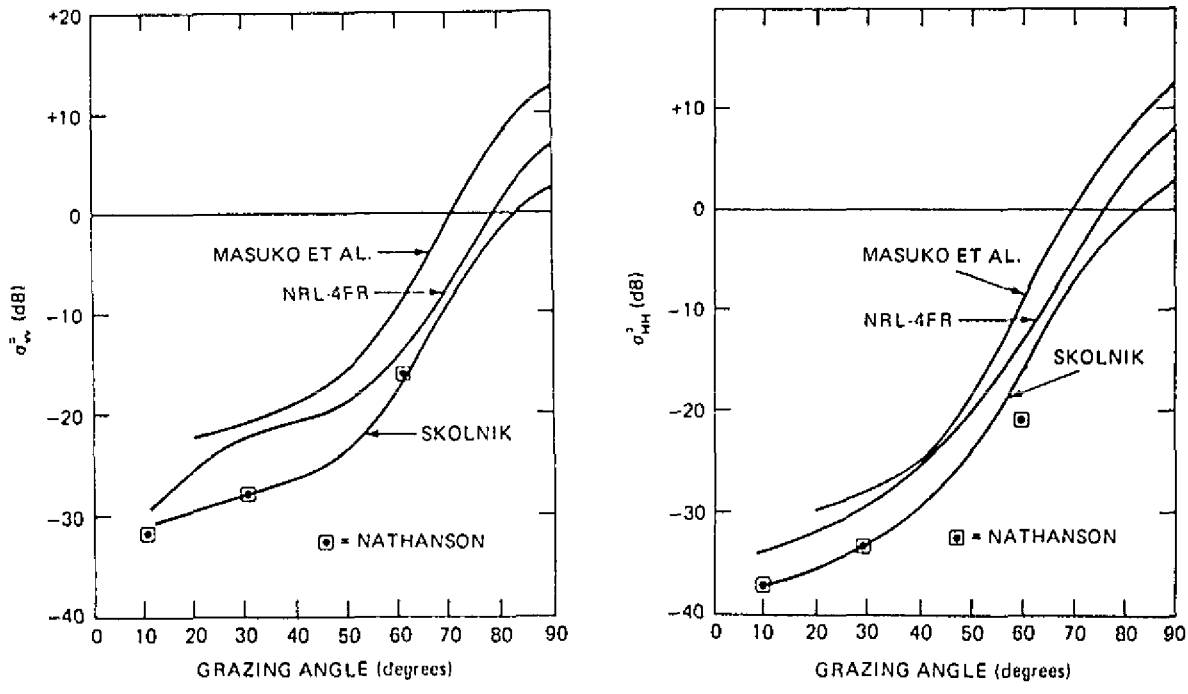

Fig. 3 — Comparison of X-band clutter data from different sources for nominal wind speed of 15 kn: (a) Vertical polarization; (b) Horizontal polarization. (Based on data from Masuko, et al, [29], NRL/4FR [21], Skolnik [2], Nathanson [3]).

(pre-1970) taken from books on radar systems by Skolnik [2] and Nathanson [3]. The discrepancies between the different data sets can be accounted for, at least in part, as follows. The older data set was based on published measurements from various sources; since wind direction is not specified, it may be assumed that it represents some kind of average of up- down- cross-wind directions. This average is 2 to 3 dB smaller than the upwind returns and is described later in this report. Moreover, the early NRL-4FR data were used liberally in the older data summaries, and as noted above, a 3 to 4 dB difference exists between the early and later presentations of the same NRL-4FR data (the latter being used in Fig. 3). With these corrections, the curves would show closer agreement. Nevertheless, it is clear that uncritical use of published clutter data could lead two radar systems designers to choose sea clutter estimates almost an order of magnitude apart for the same conditions.

The NRL-4FR data set is unique in that no other program has reported measurements made at the same time over so wide a range of frequencies, grazing angles, and wind speeds. Figure 4 shows the trends for both vertically and horizontally polarized sea clutter over a range of grazing angles down to 5°. The curves represent the centers of ± 5 dB bands that contain the major returns for the three higher frequencies (L, C, and X bands; the UHF returns were a few dB lower) and wind speeds $\gtrsim$ 12 kn. The major differences in sea clutter for the two polarizations lie in the range of grazing angles between $\sim 5°$ and 60°, where the horizontally polarized returns are smaller. This difference is found to be emphasized at both lower wind speeds and lower frequencies. The cross sections approach each other at high angles ($> 50°$), and also for the higher microwave frequencies at low angles ($< 5°$). In fact, for grazing angles less than a few degrees moderate to strong wind speeds, several observers [1, 25, 26] have reported that at X-band and at the higher sea states the horizontally polarized returns often exceed the vertically polarized returns.

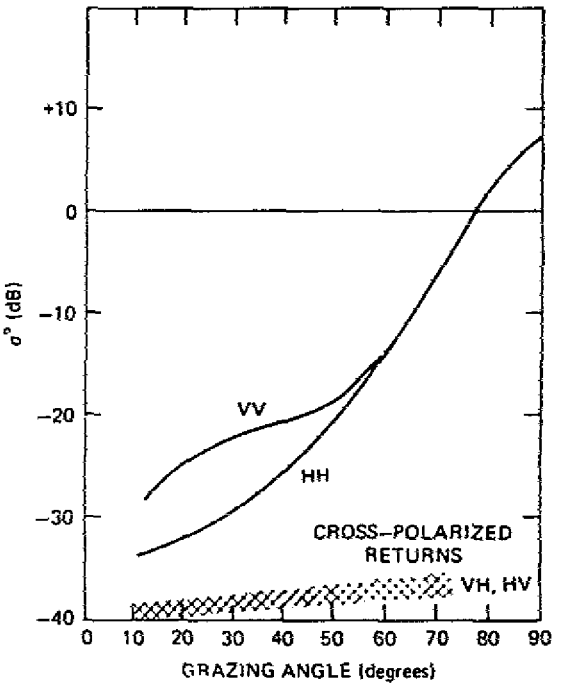

Fig. 4 — General trends in clutter behavior for average wind speeds (~15 kn) based on NRL/4FR data. Plots represent L, C, and X band data within ±5 dB.

The NRL-4FR system permitted transmission and reception on orthogonal polarizations, so data could be collected for cross-polarized sea clutter. These returns tended to have a weak dependence on grazing angle and were always smaller than either of the like-polarized returns lying in the shaded region shown on Fig. 4.

It is informative to compare measurements by different investigators in different parts of the world under similar wind conditions. Figure 5 shows measurements of vertically polarized sea clutter down to a grazing angle of 20° for wind speeds of ~15 kn from three independent experiments using airborne radars at C, X, and K band frequencies [27-29]. Although there is no assurance that all of these measurements were made over fully developed seas, clearly there is a rather strong consistency among them, which reinforces the observation made in reference to Fig. 4 that the frequency dependence of sea clutter at intermediate grazing angles is weak at microwave frequencies from L to K band.

Dependence on Wind Speed

The relationship between sea clutter and wind speed is complex and uncertain because it depends on almost all of the parameters that characterize sea clutter: frequency, grazing angle, polarization, the state of the sea surface, the direction and speed of the wind itself, and even on whether the measurements are made from an aircraft or a tower platform [31].

A common way to organize clutter data is to seek the best straight-line fit (linear regression) between clutter cross sections in dB and the log of the wind speed (or some other parameter). This, of course, *imposes* a power-law relation between the variables: $\sigma^0 \propto U^n$, where n is determined by

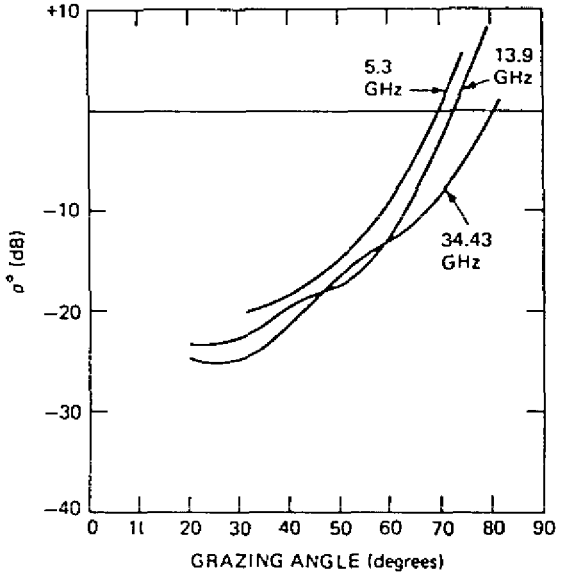

Fig. 5 — Frequency dependence of sea clutter for wind speeds of ~15 kn: 5.3 GHz, Feindt [27]; 13.9 GHz, Schroeder [28], 34.4 GHz, Masuko [29].

the slope of the line. Figure 6 shows an example [30]. On the other hand, the totality of the NRL-4FR results appears to show saturation for wind speeds $\gtrsim$20 kn, but the high and low-to-moderate windspeed data were collected at different times in different places under different conditions of sea surface development, and discrepancies between the two data sets for common wind speeds have weakened the evidence for saturation [32]. Other investigators deny that it is even possible to express the wind dependence in the form of a power law, proposing the existence of a kind of threshold wind speed, below which clutter virtually vanishes and above which the clutter level rises toward a saturation value [18]. This is indicated by the curves in Fig. 7, where the straight lines correspond to various power laws. Once this possibility is raised, examples of data can be found that appear to track such a curve while at the same time yielding a power law by linear regression. This is illustrated by the tower data shown in Fig. 8 [30]. This behavior is not uncommon.

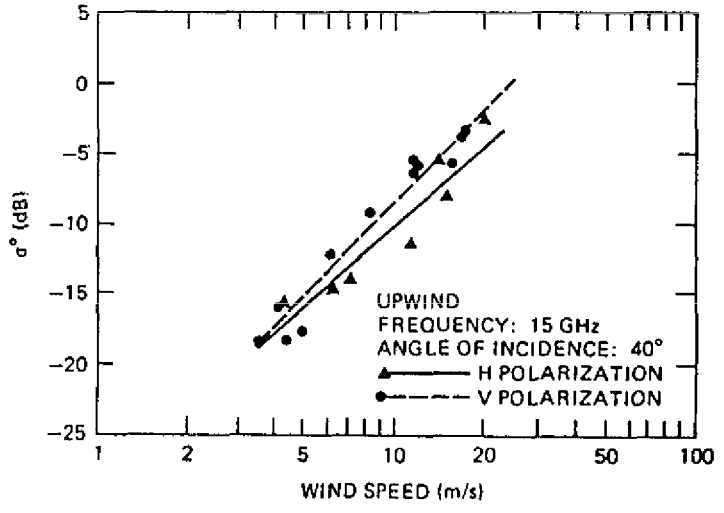

Fig. 6 — Sea clutter from a tower platform with power-law wind speed dependence defined by linear regression. (From Chaudhry and Moore [30], © 1984 IEEE).

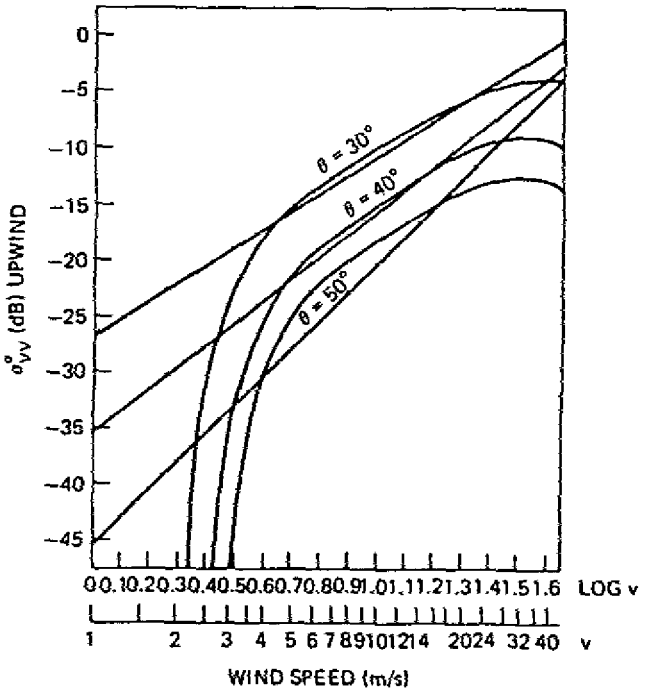

Fig. 7 — Hypothetical wind speed dependence of sea clutter (curved traces) compared with various power laws (straight lines). (Derived from Donelan and Pierson [18]).

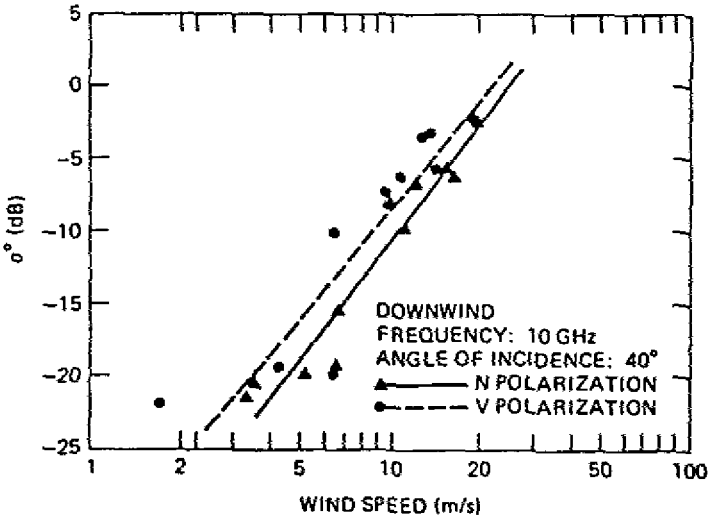

Fig. 8 — Example of forcing a power-law fit (Compare data with curves in Fig. 6). (From Chaudhry and Moore [30], © 1984 IEEE).

Nevertheless, the imposition of a power-law relation provides a convenient way to visualize trends in the behavior of sea clutter with wind speed. The various aircraft measurements referred to above [27-29] as well as data from a tower in the North Sea [30, 31], were all treated in this way, yielding plots of σ^0 as a function of wind speed and grazing angle of the form shown in Fig. 9. Plots of this type give information about both the wind speed and grazing angle dependence of sea clutter for a given frequency, polarization, and wind direction. Figure 9 is based on a blend of RADSCAT data at 13.9 GHz [29] and measurements by Masuko, et al., at 10 GHz [29], both for upwind directions. Thus they can be viewed as representative of clutter behavior in the vicinity of X-band, since the difference between the two frequencies is small. However, examination of the data points underlying these linear regressions shows point scatter that sometimes resembles Fig. 6, sometimes Fig. 8, sometimes neither, so the straight lines in these figures cannot be taken too seriously. In fact, it appears that there is no simple functional dependence of sea clutter on wind speed that can be established with any confidence from existing data. However, most investigators would probably agree that the behavior of microwave sea clutter with wind speed at intermediate grazing angles can be roughly described as follows: for light winds (<6 to 8 kn) sea clutter is weak, variable, and ill-defined; for intermediate winds (12 to 25 kn) it can be described roughly by a power law of the type found in Fig. 6; for strong winds ($\gtrsim 30$ kn) there is a tendency for it to level off. In fact, the convergence of the lines in Fig. 9 with increasing wind speed suggests that the reflectivity of the sea surface is tending toward Lambert's Law, for which there is no dependence on grazing angle, frequency, or polarization, but only on surface albedo.

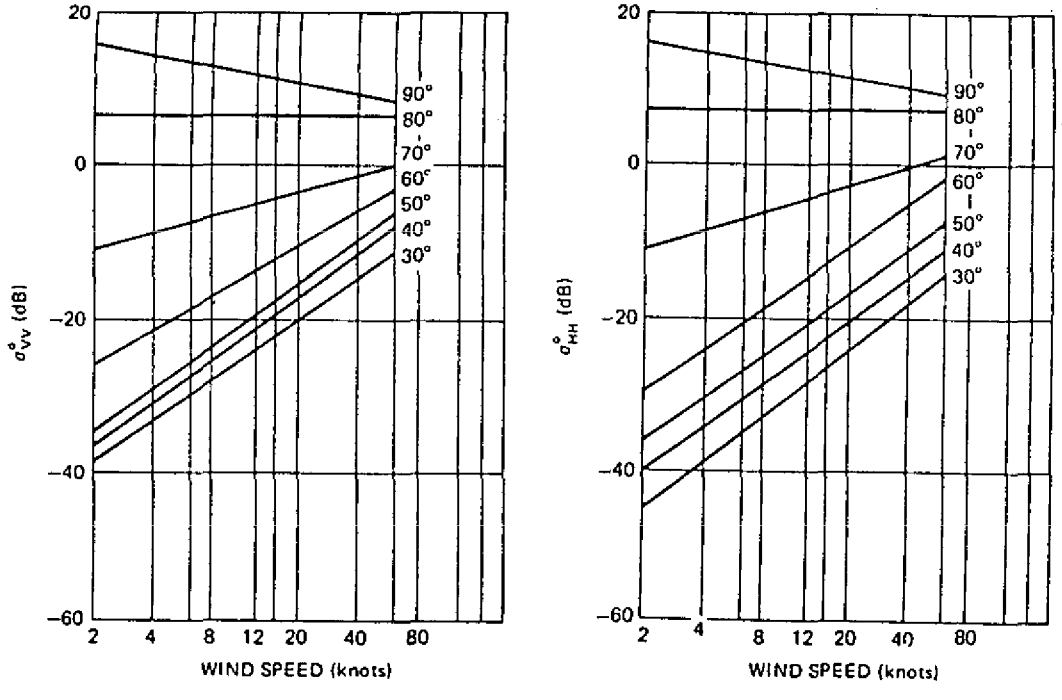

Fig. 9 — Example of clutter behavior with wind speed and grazing angle—average of data at 10 GHz [29] and 13.9 GHz [28]: (a) Vertical polarization; (b) Horizontal polarization.

Dependence on Wind Direction

In several of the referenced experiments, the dependence of sea backscatter on angle relative to the wind direction was found by recording the radar return from a spot on the surface while flying around it in a circle. Figure 10 gives an example of this behavior for grazing angles of $\sim 45°$ and wind speeds close to 15 kn [29]. The figures contain results obtained independently by three different groups. The behavior shown here is representative of that found generally: sea clutter is strongest when viewed upwind, weakest when viewed crosswind, and of intermediate strength when viewed downwind—the total variation being ~ 5 dB.

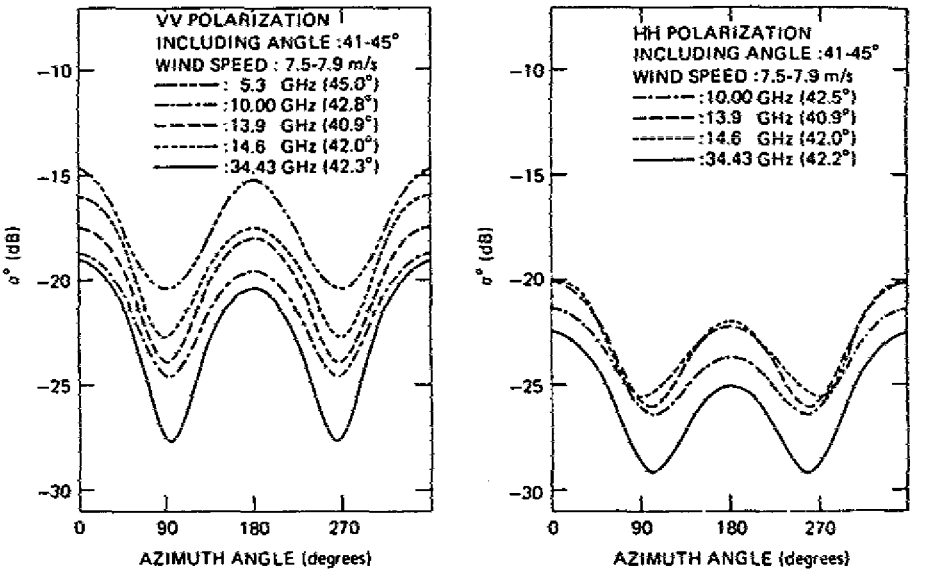

Fig. 10 — Dependence of clutter on wind direction: nominal wind speed 15 kn, grazing angle 45°. (From Masuko et al [29], © by the American Geophysical Union)

At High Grazing Angles

The top curve in Fig. 9 corresponds to clutter at a grazing angle of 90°, that is, for a radar looking straight down. On a strictly empirical basis, the clutter cross section at this angle is only weakly dependent on frequency, has a maximum of $\sim +15$ dB at zero wind speed (at least for the antenna beamwidths and experimental configurations reported), and falls off gradually as the wind picks up. Scattering at high grazing angles is commonly regarded as a form of specular scattering from tilted facets of the surface. It is of interest to note, then, that there appears to be a small range of angles in the neighborhood of 80° for which the cross section is almost completely independent of wind speed. Because these angles correspond to complements of the common rms sea slope angles of $\sim 10°$, it might be argued that as the wind increases, the decrease of clutter because of increasing surface roughness is balanced at these angles by an increase of clutter because of an increasing population of scattering facets. This line may therefore be regarded as the boundary separating the *specular* regime (where the cross section is decreased by surface roughness) from the *rough surface* regime (where the cross section increases with surface roughness). Note further that clutter measurements at these high grazing angles will be relatively sensitive to the averaging effects of wide antenna beamwidths, which could become a source of ambiguity in aircraft measurements at the lower radar frequencies.

At Low Grazing Angles

At low grazing angles, below mean sea slope angles of $\sim 10°$, sea clutter takes on a different character. The sharp clutter peaks known as sea spikes begin to appear on A-scope presentations [1, 25, 33], and the probability distributions assume a different form [34]. Figure 11 shows the presence of sea spikes in the time histories of returns from a fixed spot, measured from a tower in the Gulf of Mexico with a high-resolution X-band radar looking into an active sea at a 1.5° grazing angle [33]. The vertically polarized returns appear to be slightly broader. Although the horizontally polarized returns are more spikey, both polarizations display the sharp bursts that are characteristic of sea clutter at small grazing angles. The peak cross sections in these records are of the order of 10 m^2 and are roughly the same for the two polarizations. This is another characteristic of sea clutter at these angles. Interestingly, the same measurements made in "calm" water looked virtually identical in every detail, except peak cross sections were now only 10 cm^2, or 40 dB less.

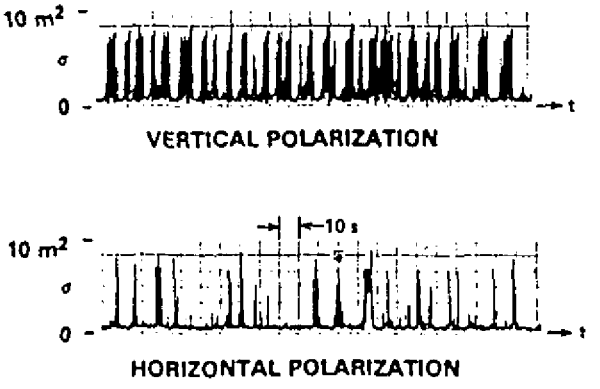

Fig. 11 — Sea spikes at X-band, 1.4° grazing angle, moderate to strong winds. Note equal amplitudes at the two polarizations and the differences in time behavior. (From Lewis and Olin [33]).

Trizna [34, 35] has accumulated a considerable body of data from measurements of low-angle sea clutter by using high-resolution (40 ns) shipboard radar in both the Atlantic and Pacific Oceans. The probability distributions of the clutter cross sections were plotted in the manner of Fig. 12, which shows the distributions of horizontally polarized X-band data at a 3° grazing angle for low, medium, and high wind speeds (in order from left to right). The low-wind trace corresponds to a Rayleigh distribution; the other straight-line segments are two-parameter Weibull distributions defined by different parameter pairs. It is clear that the behavior is different and considerably more complex than that shown in Fig. 2 for the higher grazing angles and wider pulses. Trizna interprets these distributions as follows: in each trace, the left-hand (lowest cross section) segment is actually receiver noise, recorded when the radar footprint lay in shadow; the middle section corresponds to distributed clutter, for reasons relating mainly to its weak dependence on resolution cell size; the right-hand section (highest cross sections) describe the sea spikes, for reasons relating to the dependence on wind speed (similar to whitecap dependence) and the sheer size of the components (some individual absolute cross sections are in excess of 1000 m). For the higher wind speeds and fully developed seas encountered in the North Atlantic, the population of this sea spike sector (the percentage of sea-spikes) was found to grow as the 3.5th power of the wind speed. Interestingly, this is the same wind-speed dependence shown by the percentage of whitecaps seen on the surface [36].

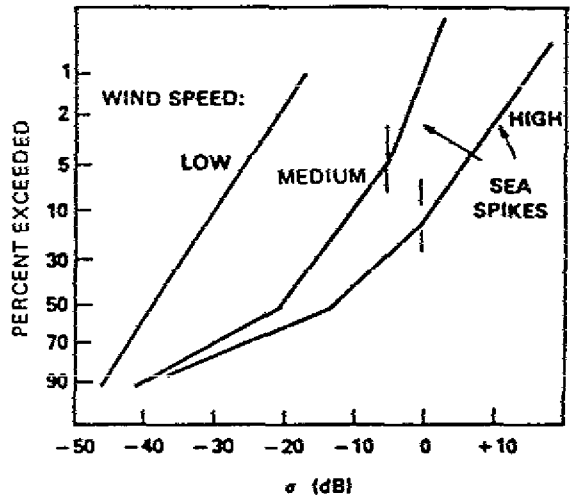

Fig. 12 — Segmented clutter probability distributions at low grazing angles (based on Trizna [34])

Remember that, to the extent that the sea surface may be viewed as a stationary homogeneous process (as it generally is over the duration and spatial extent of any particular experimental event), the scattering cross section may be said to be ergodic. This means that the statistical results obtained by time averaging from a small cell are equivalent to a shorter time average from a larger cell, provided that the number of "samples" is the same in the two cases. For this reason, the statistical implications of experimental data can be properly compared only if the details of the sampling procedure are specified. However, the number of samples in the experimental results shown thus far have been sufficiently large that the differences between, for example, Figs. 2 and 12, may be considered real, and related to differences in grazing angle rather than in resolution cell size. In fact, distributions closely resembling those in Fig. 12 were obtained much earlier from similar measurements with considerably broader pulsewidths [35].

At Very Low Grazing Angles

There is some evidence that sea clutter might drop off more sharply below a *critical angle* in the neighborhood of a degree or so (see Long [1]). This critical angle, or *critical range* for a radar at a fixed height, has been observed from time to time since first noted in early observations of sea clutter [4]. According to Katzin [37], the critical angle occurs as a result of interference between direct and (perfectly) reflected rays at the scattering *targets* responsible for the clutter signal. Although this simple picture can account for the R^{-7} decay sometimes observed, a critical angle often fails to materialize. When it does, it sometimes does not show the R^{-7} decrease with range (or the equivalent 4th power dependence on grazing angle) [1]. Wetzel [38, 12] for suggested an alternative explanation for this behavior that is applicable at the higher microwave frequencies. This explanation is based on a *threshold shadowing* model for upwind and downwind directions that implies a sharp decrease in the average cross section for grazing angles below a few degrees. In crosswind directions with the radar looking along the troughs of the major waves, a much milder shadowing function applies, so there should be a clear distinction between the upwind/downwind and crosswind behavior of sea clutter at very low grazing angles.

Examples of clutter behavior at these angles are found in independent measurements at relatively high wind speeds made by Hunter and Senior off the south coast of England [39] and by Sittrop off

the west coast of Norway [40]. Figure 13 shows their results for orthogonal directions relative to the wind, together with predictions of a conventional shadowing function [41], the threshold shadowing function [12], and the 4th-power grazing angle behavior predicted by the interference hypothesis. A combination of conventional shadowing, which goes as the first power of the grazing angle, across the wind and threshold shadowing in up and downwind directions appears to account for the observed behavior of this very-low-angle clutter quite well. The decay law for low-angle clutter should therefore depend on viewing angle relative to the wind direction, so it might occur with powers between the 1st and the 4th. This is just what is observed [42]. However, shadowing at low grazing angles is a complex phenomenon (see below), and the physical origin, or even the existence, of a critical angle is still open to question. Moreover, relatively little good data exist on very low angle clutter for other than X-band frequencies, so the general behavior of sea clutter in this angular regime remains uncertain.

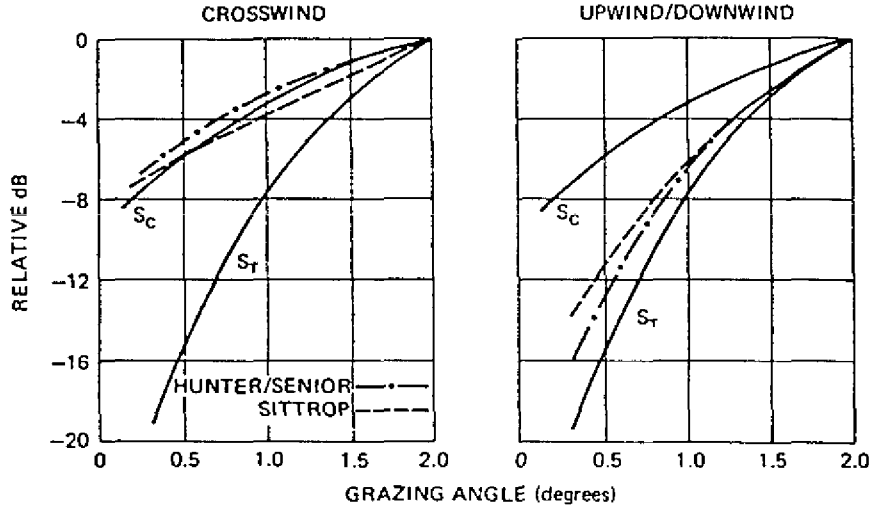

Fig. 13 — Differential behavior of very low angle clutter for orthogonal wind directions: S_c is a conventional shadowing function [41]; S_T is a threshold shadowing function [38] (data from Hunter and Senior [39] and Sittrop [40])

At HF and mm-Wave Frequencies

All of the measurements described were made at *microwave* frequencies between UHF (428 MHz) and Ka-band (35 GHz). HF radars usually operate in the frequency range between ~5 and 30 MHz, corresponding to wavelengths between 60 and 10 m, respectively. Since the operation of such radars takes place either by the ground wave, or over ionospheric (*skywave*) paths spanning great ranges, the grazing angles tend to be small (between 0° and 20°.) For these wavelengths and grazing angles, initial measurements by Crombie [5] indicated that the scattering from the sea surface was the result of Bragg scatter from sea waves of one-half the radar wavelength. In the years since these early measurements, there has been considerable activity in the field of HF radar and HF clutter [43, 44]. The results can be summarized as follows: For vertical polarization, the major energy of the HF clutter signal appears in spectral lines displaced to either side of the carrier frequency by the frequency of sea waves that have a wavelength equal to half the HF wavelength λ (meters). The relative strengths of the plus and minus lines are determined by the proportion of advancing and receding Bragg resonant wave components in the clutter cell. Provided the windspeed is greater than about $(3\lambda)^{1/2}$ kn (with λ in meters) and the sea is fully developed, the clutter cross section σ^0 is ~ -27 dB,

and is relatively independent of wind speed and frequency. (The definition of σ^0 in HF radar is complicated by problems in properly defining antenna gains for groundwave and skywave paths and by propagation effects caused by the ionosphere.) The clutter spectrum tends to fill in around and between the lines as the wind picks up. For horizontal polarization (which is possible only over skywave paths), the cross section is much smaller and shows the characteristic fourth-power decay with decreasing grazing angle. For these HF wavelengths of tens of meters, the sea is relatively flat, and the scattering laws are simple.

At the other end of the potentially useful radar spectrum, in the millimeter-wave band, the few published measurements of radar clutter lead to the conclusion that millimeter wave backscatter behaves in much the same manner as backscatter at the lower microwave frequencies. This is suggested by the K-band curves shown in Fig. 5 for moderate wind speeds and further supported by some older shipboard data at frequencies between 9 and 49 GHz [45]. Note that clutter signal paths lie close to the sea surface where the atmospheric and water vapor densities are highest. This means that at these higher frequencies the clutter signal is strongly affected by the atmospheric absorption effects described previously. Consequently, the surface-related cross section inferred from the received signal strength in any given measurement depends on the path length. Moreover, the role of sea *spray* in both scattering and absorption is certainly more important than at the lower microwave frequencies.

It is difficult to find clutter data at frequencies above K_a band, although H- and V-polarized returns at 95 GHz at a grazing angle of 1° were reported, both with values of σ^0 close to −40 dB [46, 47]. Interestingly, this is the same cross section measured at X-band for this angle by a number of investigators [12] showing a similarity between the returns at these two widely spaced frequencies. However, at lower frequencies, at L band and below, there is a noticeable tendency for the cross section to fall off with decreasing grazing angles below $\sim 15°$ to 20°.

THE SPECTRUM OF SEA CLUTTER

The scattering features that produce sea clutter are associated with a surface subject to several types of motion. The features may themselves be moving with small group or phase velocities over this surface while the surface, in turn, is moved by the orbital velocities of the larger waves passing across it. Or the scatterers might be detached from the underlying surface, as in the plumes emitted at the crests of breaking waves, and move at speeds much greater than the orbital speeds [48]. At higher radar frequencies and in strong winds, the possibility of scattering from spray, advected by the wind field above the surface, must be considered. All of this complex motion shows up in a Doppler shift imparted to the scattered electromagnetic wave.

Surprisingly few measurements of microwave clutter spectra for real seas have been reported in the literature. The few that do exist can be separated into aircraft measurements of the spectral shape alone [49, 50] and fixed-site shore measurements showing a shift in the spectral peak [51, 52]. All of these studies were performed at relatively low grazing angles ($< 10°$), although Valenzuela and Laing include a few measurements up to 30°. Other measurements of sea clutter spectra include those made at much lower frequencies in the HF band, (described in the previous section), those made under artificial conditions in the wave tank [53] whose application to real sea conditions is uncertain, and other fixed-site measurements at high resolution and short averaging times (to be discussed later).

Microwave sea clutter spectra have a rather simple form at the lower grazing angles. Figure 14 illustrates typical spectral behavior at the two polarizations for C-band clutter looking upwind at a few degrees grazing angle based on data collected by Pidgeon [51]. The peak frequency of the upwind

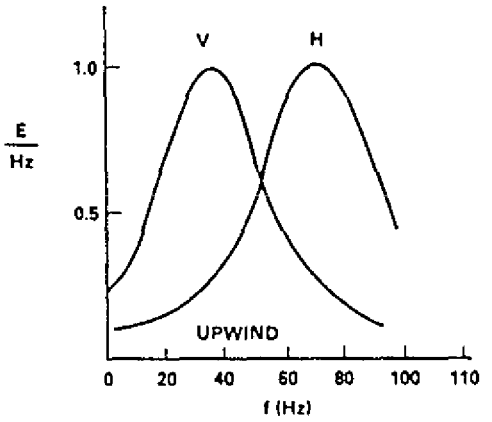

Fig. 14 — Qualitative behavior of doppler spectra of sea clutter looking upwind at low grazing angles (based on C-band measurements by Pidgeon [51])

spectrum appears to be determined by the orbital velocity of the largest sea waves. It also includes a wind-dependent velocity increment that contains but is not entirely explained by wind-induced surface currents. The orbital velocity V_{orb} is taken to be that of the major waves and is obtained in terms of significant height $H_{1/3}$ and period T from the expression

$$V_{orb} = \pi H_{1/3}/T \simeq 0.1\ U. \tag{10}$$

The approximate dependence on wind speed U was found by substituting $H_{1/3} = 3h_{rms}$ from Eq. (6) (assuming a fully developed sea), and T from Eq. (5). To this must be added a wind-drift velocity of $\sim 3\%$ of U and a fixed *scatterer* velocity (which appears to be $\sim .25$m/s in the X- and C-band measurements [51, 52, 54].) Summing these components yields the virtual doppler velocity at the peak of the clutter spectrum for the particular case of a *vertically polarized, X or C band* radar looking *upwind* at *low grazing angles*:

$$V_{vir} \simeq 0.25 + 0.13\ U \text{ m/s}. \tag{11}$$

(As noted earlier, care must be taken whenever wind speed is used to parameterize a process that depends on wave height. An unambiguous relationship exists only for a fully developed sea in the absence of swell.) The remaining properties of the clutter spectrum can now be discussed in terms of V_{vir}. For example, the spectral peak for *horizontal* polarization follows a similar linear dependence on U, except with a coefficient lying somewhere between 0.17 and 0.20, as may be noted in Fig. 14. The (half-power) width of the clutter spectrum is roughly the same for both polarizations and is equal approximately to the upwind vertical velocity given in Eq. 11. For look directions away from upwind, the peak doppler follows a cosine dependence very closely, going to zero at crosswind aspects and turning negative downwind. Interestingly, the *bandwidth* of the spectrum remains relatively constant.

The details of the clutter spectrum show little dependence on either the radar frequency or the grazing angle, at least for angles $\lesssim 10$. In reviewing the results of measurements at four frequencies—UHF, L, C, and X bands—Valenzuela and Laing [50] noted a relatively weak tendency

of clutter bandwidth to decrease with increases in frequency between the UHF and X bands and grazing angles between 5° and 30°. Since both of these variations entail a decrease in the size of the radar footprint on the surface, they could be due to a dependence on resolution cell dimensions, although the other workers found that the pulse length had little effect on clutter bandwidth for values between 0.25 and 10 μs. The equivalence between time and space averaging in sea clutter measurements was discussed earlier. For clutter spectra, the averaging times were all quite long (of the order of 10 to 20 min), which should be sufficient to stabilize the spectra for almost any resolution cell size.

Spectra obtained with short averaging times disclose something of the origins of the clutter spectrum. Figure 15 is a sequence of 0.2^{-s} spectra obtained by Keller et al. [55] with a coherent vertically polarized X-band radar operating at a grazing angle of 35° and resolution cell size of ~ 10 m. The zero-doppler reference in this figure was located arbitrarily at -16 Hz; because of the high grazing angle, the effects of both senses of the orbital velocities are seen, unlike the low-angle shadowed surface results shown in Fig. 14. The spread along each line is due to the small-scale wave motions on the surface. The larger meanders are induced by the orbital velocities of the large waves moving through the measurement cell. The wind speed was 16.5 m/s, and a doppler shift of 100 Hz corresponds to a radial velocity of 1.6 m/s. The average clutter spectrum expected for this wind speed and grazing angle, with bandwidth obtained from Eq. (11), is sketched on the figure. The large spectral spike appearing in the center of the display is no doubt due to a wave breaking in or close to the measurement cell. The doppler velocity for this spike suggests a peak scatterer velocity of about half the wind speed. This speed would correspond to the group velocity of the longest waves on the surface. Although such events are relatively rare in a fixed area of 10 m, they should occur quite frequently within a large surveillance cell and could have large scattering cross sections associated with them.

OTHER EFFECTS ON SEA CLUTTER

Rain

Evidence of the effect of rain on sea clutter is mainly anecdotal; for example, radar operators report that sea clutter tends to decrease when it starts to rain. However, very little reliable, quantitative experimental information exists about the interaction between rain and wind-driven sea scatter. Laboratory measurements by Moore et al. [56] with artificial rain suggest that for light winds the backscatter level increases with rain rate, while for heavy winds rain made little difference. In measurements in natural rain over the Chesapeake Bay, Hansen [57] found that even a light rain (2 mm/h) changes the spectral character of sea clutter at moderate wind speeds (6 m/s) by introducing a significant high-frequency component. He also found some evidence in support of the radar operators, at least for the low grazing angles and horizontal polarizations with which most shipboard radars operate. Figure 16 compares the correlation function of sea clutter (X-band, low grazing angle, H-polarization) with and without rain for a 15-kn wind speed and a rain rate of 4 mm/h. The sharp decrease in correlation time in the presence of rain reflects the broadening of the clutter spectrum. Beyond this very little quantitative information is available concerning the effect of rain on existing sea clutter.

The production of sea clutter by rain falling on a calm surface in the absence of wind was also investigated by Hansen [57]; the results are shown in Fig. 17. A high-resolution X-band radar (40 ns pulse, 1° beamwidth), operating at a grazing angle of $\sim 3°$, viewed the backscatter from a fixed spot

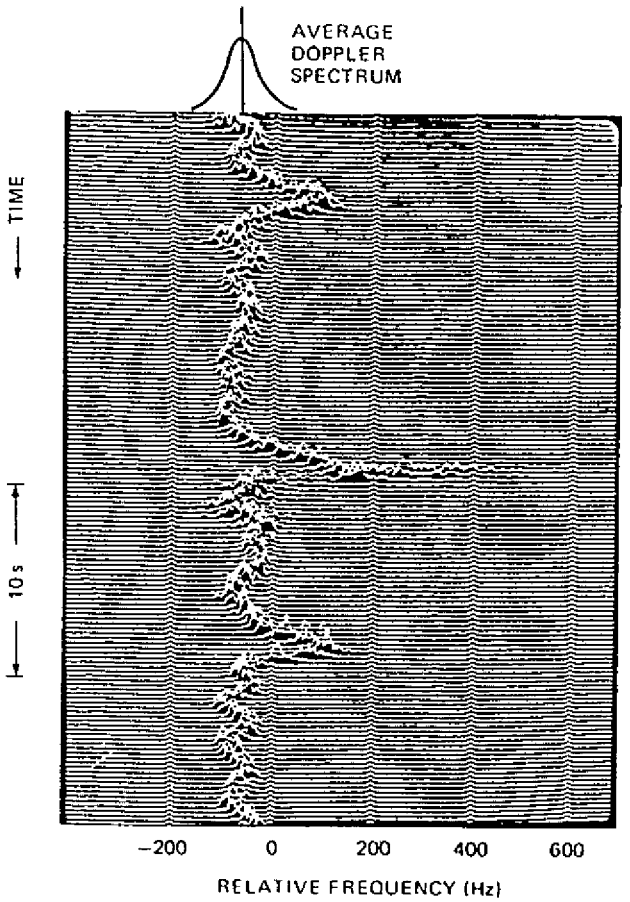

Fig. 15 — Short-time averaged doppler spectra at X-band for an intermediate grazing angle of 35°; spectra computed at 0.2 s intervals (from Keller et al [55])

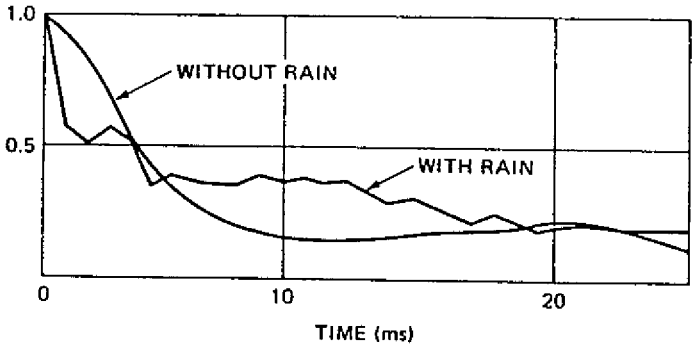

Fig. 16 — Effect of rain on the correlation function of wind-driven sea clutter; X-band, horizontal polarization, wind speed 15 kn, rain rate 4 mm/h (from Hansen [57])

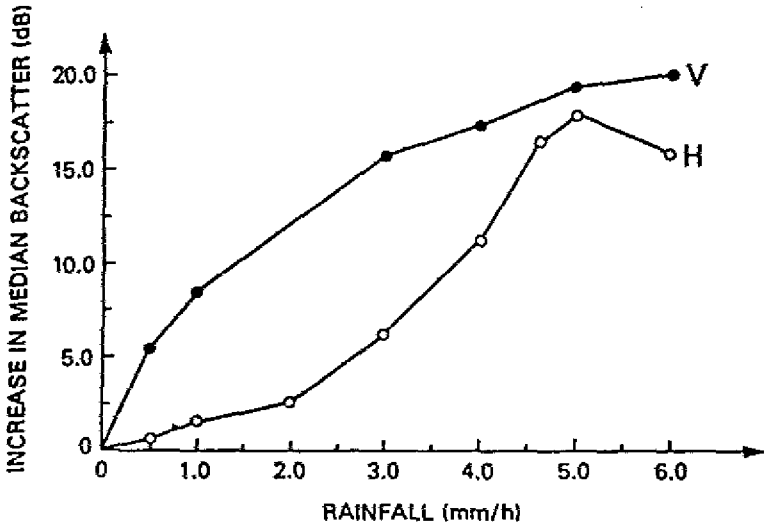

Fig. 17 — Sea clutter produced by rain splashes alone on a calm surface (from Hansen [57])

on the windless surface of the Chesapeake Bay as the rain steadily increased from 0 to 6 mm/h. The cross sections for vertical and horizontal polarizations were quite different for low rain rates but tended to merge at a rain rate of ~6 mm/h. The magnitude of this *splash* cross section rose to $\sigma^0 \simeq -40$ dB, corresponding to wind-induced cross sections at this grazing angle for winds of ~10 knots. Further laboratory [58] and theoretical [59] studies have shown that the major scattering feature is the vertical *stalk* that emerges shortly after drop impact. Moreover, these studies suggest that the V-polarized returns from raindrop splashes should be relatively insensitive to rain rate, while the H-polarized returns should show a strong dependence on both the rain rate and the drop size distribution.

Propagation Effects

Another largely unexplored topic in sea clutter is the role played by propagation effects within the atmospheric boundary layer just above the sea surface. The effects of atmospheric absorption have been noted above in connection with mm-wave clutter. However, at very low grazing angles the ray paths joining the radar to the surface become very sensitive to refractive inhomogeneities in the atmospheric boundary layer. Over distances approaching and beyond the conventional optical horizon, these perturbations could produce strong focus-defocus variations along the illumination profile [60] or a general rise in the local grazing angle [38]. Figure 18 gives an experimental example of the effect of ducting on very-low-angle sea clutter [42]. Since the grazing angle given as the abscissa is actually a plot of inverse range, the lifting of the cross section by ducting over an order-of-magnitude span of ranges is very likely due to a rise in the mean grazing angle produced by refraction in the evaporative layer [38]. Such effects should be suspected whenever the radar propagation path extends beyond the *optical* horizon.

Shadowing

The possibility of shadowing must be seriously considered whenever the sea is viewed at grazing angles smaller than the rms slope angle of the sea surface. Some examples were discussed earlier in connection with the behavior of sea clutter at low grazing angles shown in Fig. 13. In fact, the sharp fall-off of the *nonducting* data in Fig. 18 gives further evidence of the *threshold shadowing* mentioned

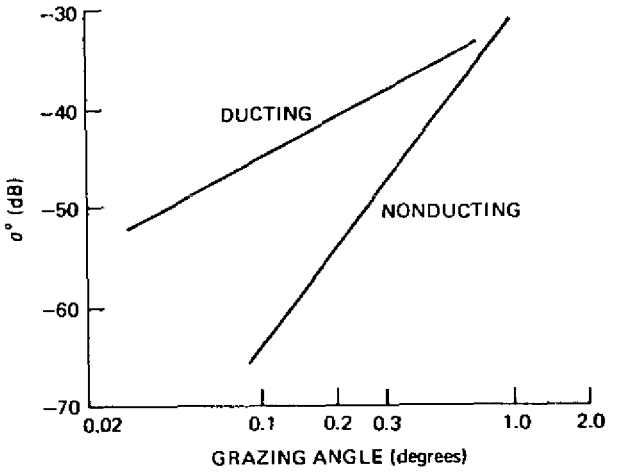

Fig. 18 — Effect of ducting on low-angle clutter; wind speed ~10 kn
(based on data in Dyer and Currie [85])

there. However, the common idea of shadowing, together with all existing theories of a shadowed surface, rests on the geometrical optics concept of a sharp transition between light and darkness. By considering the implications of diffraction at the wave peaks, it is possible to determine the domain of radar frequencies and wind speeds over which the concepts of geometrical optics may be applied. This was done by Wetzel [12], who showed in detail how diffraction, rather than shadowing, controls propagation into and out of the troughs of the waves under many of the usual frequencies and windspeeds encountered in practical radar operations at low grazing angles. For example, shadowing will take place at K_a band for any winds >15 kn yet will hardly ever occur at L-band frequencies.

Contaminants

The idea of "pouring oil on troubled waters" is a familiar one; the angry surface will smooth and subside. In another age, the survival gear locker of every sailing ship would contain a bottle of oil to quiet the sea in a storm. Although the effectiveness of this procedure has always been somewhat controversial, there is no question that oil can produce a *slick* of smooth water at relatively low wind speeds. In fact, biological oils, produced by bacteria, algae, and plankton, can be found everywhere on the world's oceans and form natural slicks in those regions that combine the greatest oil concentration with the lowest wind speeds, e.g., close to continental shorelines [61]. Manmade contaminants can, of course, have the same effect. A layer of oil only one molecule thick will significantly affect the ability of the surface to support wave motions, but this layer must be continuous. The adjacent molecules then sense each other and form a film that is resistant to horizontal compression. The surface elasticity is changed, a type of longitudinal viscosity is introduced, and the surface becomes stabilized against the growth of short waves up to several inches in length [62, 63].

To the extent that radar sea clutter is produced by small-scale surface roughness (at grazing angles $\lesssim 80°$), the presence of oil on the surface should lead to a measurable decrease in clutter cross section. But as noted above, the reduction of small wave motions requires the existence of a *continuous* monolayer; slick formation is a go or no-go process, so slicks will tend to have relatively sharp boundaries. In operating the NRL 4FR system as a synthetic aperture radar to obtain images of the slicks produced by oil spills, Guinard found that the slicks were well defined, that it took very little oil to maintain a visible slick, that vertical polarization provided much greater contrast than did horizontal, and that the slicks were quenched by winds and currents [64]. Although signal strength was

not recorded in this imaging experiment, later measurements at X and L band by others [65] indicated that at the higher grazing angles ($\sim 45°$) the clutter reduction produced by the types of oil occurring in natural slicks was rather small, of the order of a few tens of percent. Since slicks are dispersed by the wind and associated wave action at wind speeds $\gtrsim 10$ kn, the effect of natural slicks on clutter may not be clear because they tend to occur in the regime of low windspeeds where the sea surface is already ill-defined.

The celebrated *sun glitter* measurements by Cox and Munk [66] gave a quantitative measure of the effect of contaminants on the surface slopes in open water, showing that the wind-generated component of the rms slope of *oiled* waters is significantly smaller than that of "clean" water. The heavy man-made oils used in their experiment were effective in suppressing small-scale waves over a range of wind speeds well beyond those that would normally disperse the lighter natural oils, so the effect of oil spills on sea clutter should be expected to extend to the higher wind speeds. In fact, at these higher wind speeds the depression of radar backscatter by such oils at X and K_a band can reach 10 to 20 dB at intermediate grazing angles between 30° and 60° [92, 93].

Currents

The most obvious effect of a current on sea clutter would be a shift in the peak of the doppler spectrum, similar to the contribution of the 3% wind-drift current mentioned in connection with Eq. (8). Another effect is related to the fact that the excitation of the surface-wave system depends on the apparent wind, so significant differences can occur in wave height, depending on whether the wind is blowing with or against the current. According to Eq. (6), the wave height is proportional to the square of the wind speed. For example, in the Gulf Stream with a current of 4 kn flowing north, a 15 kn northerly wind blowing against the current will raise a sea three times as high as a 15 kn southerly wind blowing with the current. Even with no wind, the presence of strong current shears can produce highly agitated surfaces. Shipboard observers have reported bands of roaring breakers passing by on an otherwise smooth surface, presumably produced by powerful surface-current shears associated with large-amplitude internal waves [67]. In a more subtle way, currents are thought to be responsible for SAR images that contain the expression of bottom topography in shallow waters [68]. In each of the examples cited, the current produces a change in the surface roughness that can be expected to produce a change in sea clutter cross section.

Combined Effects

Some idea of the complexity within a clutter scene resulting from *other effects* can be obtained from Fig. 19, which is a digitized PPI display of clutter in the Sargasso Sea, under light wind conditions, near a thermal oceanic front [69]. Although all of the possible contributing effects were not identified, observers noted the presence of man-made detritus organized by the currents at the edge of the thermal front, slicks probably of both natural and artificial origin, fronds of seaweed close to the surface, and the presence of light and variable winds. The dynamic range of the digitized (false-color) PPI was 30 dB, and some of the clutter contrasts, across what are obviously extremely sharp boundaries, were almost this great.

THEORIES OF SEA CLUTTER

The sea surface is so rich in potential scattering structures that in seeking to understand the phenomenology experimenters and theorists alike have proposed, and have found support for, almost any imaginable model. Aside from providing an intellectual basis for "understanding" sea clutter phenomena, however, a theory of sea clutter should serve the practical purpose of providing accura

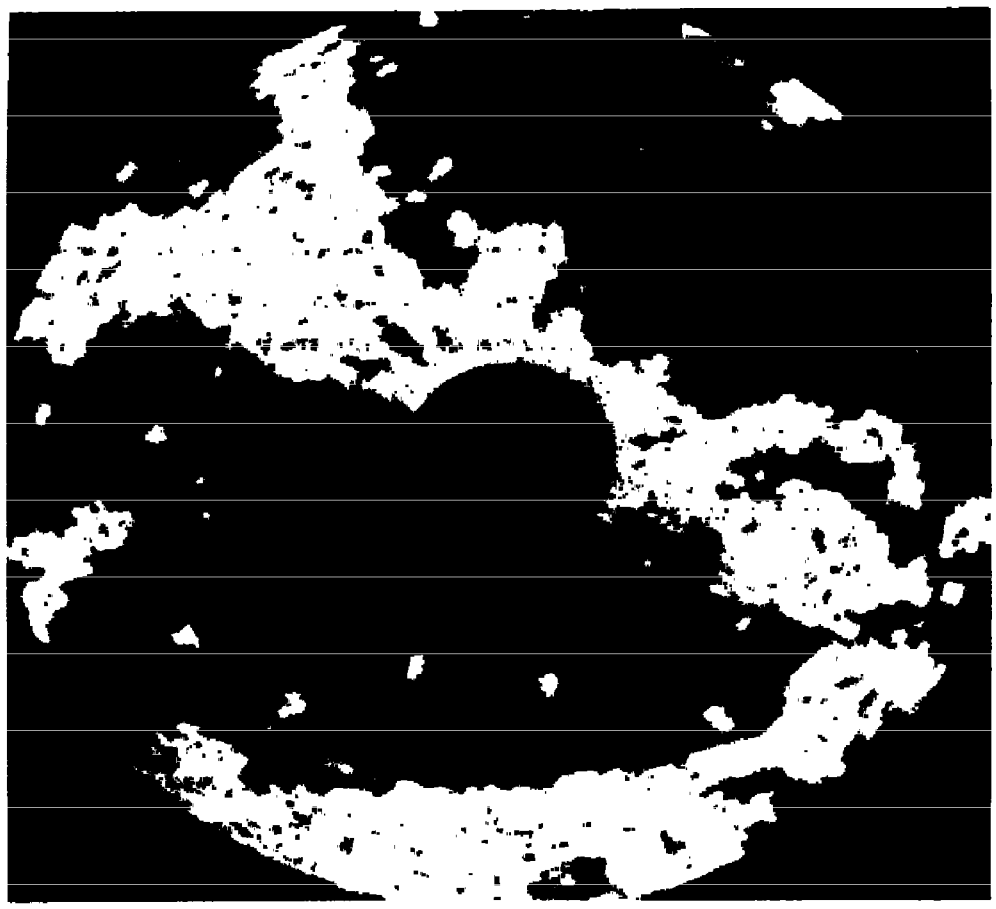

Fig. 19 — Example of strong clutter contrasts under special environmental conditions; light winds in the Sargasso Sea (provided by Trizna [69])

iori predictions of all aspects of clutter behavior under all possible environmental conditions. At ent, the Theory of Sea Clutter does neither of these tasks very well and must be thought of as a with the final chapters still to be written.

Before discussing the current theories of sea clutter, it is important to distinguish them from r so-called sea clutter *models* that are designed to provide a predictive capability. Some such els organize large quantities of empirical data by finding a multiple linear-regression formula the clutter cross section to a variety of parameters, such as grazing angle, wind speed, fre- y, etc., all measured concurrently [1, 40]. Even a multiparameter matrix tabulation of the aver- values of all available data can be viewed as a "model" [3]. Data summarized in this way can be useful to the system designer in establishing ballpark estimates of clutter levels under various ons. However, it is of little use for real-time predictions in a dynamic environment or for pro- a basis for a physical understanding of sea backscatter.

In developing models of sea backscatter based on physical theory, there are essentially two , and distinct, approaches. Historically, the first approach assumed the clutter return to have its in scattering *features*, or obstacles, actually present on or near the sea surface. For example, ing to explain the difference between the cross sections for the two polarizations, Goldstein [70] ed a kind of "rain" model to the cloud of spray often seen above the surface of an active sea, he failed to explain why the difference was the same whether or not spray was present. At least was an observable feature of the sea environment. Later features included smooth circular discs [37, 71], arrays of semi-infinite planes [72], and fields of hemispherical bosses [73], to a few. Obviously, the choice of these scattering obstacles related more to the preexistence of ient scattering solutions for these shapes than to insights gained from observing the sea. More y, feature models have taken on a bit more reality by focusing on wedge shapes, as suggested

by the Stokes waves and sharp crests observed on most natural water surfaces [12, 25, 74, 75], and by the *sloshes* and *plumes* suggested by the properties of wave groups and the hydrodynamics of breaking waves [12, 48].

The other approach to theoretical modeling derives the scattered field from a global boundary-value problem (GBVP) in which the sea as a whole is considered a boundary surface whose corrugations are described by some kind of statistical process. An enormous literature is devoted to the theory of surface scatter from this point of view, stemming from the importance not only of radar sea scatter but also from radar ground scatter and sonar *reverberation* (the acoustic equivalent of radar clutter) from both the surface and bottom of the sea. Since the GBVP approach leads to the analytical expression of Bragg resonance scattering that has dominated the theory of sea backscatter since the late 1960s, a brief explanation of some of the central ideas is included below.

Theories Based on Global Boundary-Value Problems

Unfortunately, general formulations of the GBVP, although elegant, are of little practical value, and some kind of approximation is necessary to obtain useful quantitative results from them. The methods of approximation relate to the two methods of formulating the GBVP:

(1) Small-amplitude approximations (sea wave heights much smaller than the radar wavelength) are used with Rayleigh's hypothesis, in which the boundary conditions are used to match a spectrum of outgoing plane waves to the incident field [8, 76-78], or

(2) A general integral formulation based on Green's Theorem is pursued either in a small-amplitude approximation [5, 6, 79] or under the assumptions of physical optics (surface curvatures much greater than the radar wavelength) [80-82].

In formulation (1), sometimes called the "small perturbation method" (SPM) and associated most often with the work of Rice [8], the surface displacements are assumed everywhere to be much smaller than the radar wavelength. Therefore the method is directly applicable only to cases such as HF scattering, with wavelengths of tens of meters, at low to intermediate wind speeds, and with wave heights of a few meters at most. The solution is in the form of a power series in the ratio of sea wave height to radar wavelength. It predicts the first-order Bragg lines and second-order spectral filling around the lines that was mentioned in the earlier section on HF sea clutter.

On the other hand, the various integral formulations referenced above are usually formulated in very general terms. In most of them, however, σ^0 either appears in, or can be put into, a form represented schematically by the following simplified one-dimensional expression (see Ref. 10 or Ref. 80, for example):

$$\sigma^0(\psi) = Ak^2 F_p(\psi) \int_{-\infty}^{+\infty} dy\, e^{i2k_1 y} \left[e^{-4k_2^2 h^2 [1 - C(y)]} - e^{-4k_2^2 h^2} \right] \tag{12}$$

Here A is a constant, $k_1 = k \cos \psi$, and $k_2 = k \sin \psi$, where k is the radar wavenumber $(2\pi/\lambda)$; $F_p(\psi)$ is a function of polarization p, grazing angle ψ, and the electrical properties of seawater; h is the rms sea wave height, and $C(y)$ is the surface correlation coefficient. Of course, the reduction of a complicated boundary value problem to so simple a form requires assumptions about both the surface fields and the distribution of the sea heights, which is Gaussian to a good approximation [83]. But except for the SPM approach mentioned above, where small ratios of h/λ are assumed from the

beginning, the results of virtually all of the existing GBVP theories derive from expressions resembling Eq. (12), for which there are no a priori restrictions on surface heights.

The statistical properties of the sea surface enter through the correlation coefficient $C(y)$ appearing under the integral sign in the exponential in the brackets; by expanding this exponential, Eq. (12) may be written:

$$\sigma^0(\psi) = AF_p(\psi)e^{-4k_2^2h^2} \sum_{n=1}^{\infty} \frac{(4k_2^2)^n}{n!} W^{(n)}(2k_1) \tag{13}$$

where

$$W^{(n)}(2k_1) = \int_{-\alpha}^{+\infty} d\tau\, e^{i2k_1\tau} \left[h^2\, C(\tau)\right]^n \tag{14}$$

Interestingly, back in 1963 this expression was treated in some detail in the standard reference book by Beckmann and Spizzichino for the special case of a gaussian correlation function [81]. Although it becomes analytically intractable for more general correlation functions, this expression continues to show up in papers on rough surface scattering [10, 84].

Bragg Scattering from Integral Formulations

In the limit of small ratios of rms waveheight to radar wavelength or, more specifically,

$$2kh \sin \psi << 1, \tag{15}$$

only the first term in the series in Eq. (13) survives. The cross section assumes the very simple form:

$$\sigma^0(\psi) \approx 4\, \pi\, k^4 F_p'(\psi)\, W^{(1)}(2k \cos \psi), \tag{16}$$

where the constant A has been made explicit, and F' has absorbed a $\cos^2$ term from the series. $W^{(1)}$ is the Fourier transform of the surface correlation function, which makes it the sea wavenumber spectrum (discussed in Section 2) evaluated at twice the (surface-projected) radar wavenumber, which is the *Bragg-resonant* wavenumber. Except possibly for the details of the angle factor F', Eq. (16) is equivalent to the result obtained by the SPM discussed; although it is sometimes felt that its derivation from a surface integral provides some potential for greater generalization, it carries with it all of the same restrictions.

Nevertheless, this direct, linear relation between radar cross section and the oceanographers' descriptor of the sea surface has powerfully influenced thinking about the physical origins of sea clutter. It is intuitively appealing, and it offers a simple way both to predict radar clutter from measurements or forecasts of the sea spectrum, and, inversely, to use radar backscatter measurements to provide remote sensing of the sea surface for oceanographic and meteorological applications. As noted earlier, HF radar clutter is described quite well by a Bragg model, and in fact at most wind speeds is predicted with reasonable accuracy by Eq. (16). Moreover, this relation has been exploited with great success in providing long-wavelength sea spectra from HF clutter measurements [86, 87].

At microwave frequencies, however, the small perturbation assumption on which the Bragg model rests is violated on any real sea surface. Consider, for example, an X-band radar (3-cm wavelength) looking at the sea with a grazing angle of 45°. The small-perturbation condition expressed by Eq. (15) means that the maximum departure of the sea surface from a flat plane must be much smaller than 7 mm. But for the median oceanic wind speed of 15 kn, the rms wave height is 0.3 m, making $2\,kh \sin \psi = 84$. Thus the condition for using Eq. (16) is strongly violated, and the power series in Eq. (13) would contain thousands of terms, making it essentially useless regardless of the form taken by Eq. (14). It appears, therefore, that the use of integral formulations in the practical solution of the sea clutter problem will require something more sophisticated.

Other Limiting Conditions

Instead of expanding the exponential in the integrand of Eq. (12), it should be possible, at least in principle, to replace $C(y)$ directly by the Fourier transform of $W(K)$ (the inverse of Eq. (14) for $n = 1$, thus providing a functional relationship between the radar cross section and the sea wave spectrum without the restrictions of a small-amplitude approximation. This approach involves extensive computations even to obtain limited results in individual cases, as shown in work by Holliday et al. [10]. However, one interesting result of this approach was the discovery that the importance of the Bragg-resonant part of the spectrum appeared to decrease significantly with increasing wind speeds and frequencies. This conclusion casts suspicion on the significance of Bragg scatter under conditions other than those for which Eq. (16) is valid.

In the opposite limit of large kh, another approximation is used. In this case the integrand in Eq. (12) is vanishingly small *except* for small values of y, for which the correlation coefficient $C(y)$ is close to unity. The first few terms in an expansion of $C(y)$ around $y = 0$ are

$$C(y) = 1 + C'(0)y + (1/2)C''(0)y^2, \tag{17}$$

where $C(0)$ has been put equal to 1 in the first term. For Gaussian-like correlation coefficients $C'(0)=0$ and $C''(0)=-L^2$, where L is the correlation length of the process. If Eq. (17) is substituted into Eq. (12) with these values, the resulting integral is in a standard form, and the cross section becomes

$$\sigma^0(\psi) = A' F_p(\psi)(h/L)^{-1} \exp\left[-\cot^2\psi/4(h/L)^2\right] \tag{18}$$

which says that even under *very rough* conditions in which $kh >> 1$, long, smoothly varying surfaces with small ratios (h/L) would produce very little clutter, while choppy, *noisy* surfaces with large ratios would scatter much more energetically. Unfortunately, this result has little value in making quantitative predictions of sea clutter from given environmental conditions.

If the basic integral formulation of the GBVP is solved in the physical optics approximation (large k), and the scattered field found by the method of stationary phase, the result is an expression commonly called the *Specular Return*. It is described this way because its origin can be traced to pieces of the surface that provide a reflection point for the incident wave [81, 88]. This expression is written for a Gaussian sea surface in the form:

$$\sigma^0(\psi) = (|R|^2/s^2)\csc^4\psi \exp\left[-\cot^2\psi/s^2\right], \tag{19}$$

where s is the rms surface slope, and R is the flat-surface reflection coefficient for normal incidence. This is the type of scattering alluded to in connection with the high grazing angle returns discussed in Section 3, and the tendency of σ^0 to round off for grazing angles close to 90° (see Figs. 3 and 4) can be ascribed to this mechanism.

From what has been said thus far, it can be seen that strict analytical solutions obtained from the GBVP approach appear to run into dead ends: intractable formal expressions in the form of Eq. (12), small-amplitude approximations in the form of Eq. (16) that make little sense for microwave scattering from real sea surfaces, or large-amplitude limits like Eqs. (18) and (19) that ultimately relate to the probability densities of specularly reflecting surface slopes. However, judging from the success of Holliday et al., in obtaining useful information from a numerical evaluation of the integrand in Eq. (12), quite possibly the best hope of obtaining useful results for real seas from GBVP formalisms might lie in further study of the surface-correlation function.

The Composite-Surface Hypothesis

It is not clear how to extend straightforward GBVP solutions beyond the limiting approximations described above. Therefore a heuristic model was developed that viewed the sea as a carpet of Bragg scattering wavelets obeying the condition in Eq. (15), modulated by the motions of the larger waves on the surface [6, 88-90]. It is imagined that the surface-wave spectrum can somehow be separated into two parts, one that contains the Bragg-scattering wavelets and whose integrated rms waveheight satisfies the conditions of Eq. (16), and another which contains only the long waves that tilt and otherwise modulate the Bragg waves. Other assumptions include: (1) that the correlation lengths of the short Bragg waves be long enough that a resonant interaction is possible, but short enough that adjacent areas on the surface contribute to the total signal in random phase; and (2) that the long waves that tilt and modulate the short waves have radii of curvature sufficiently large that the curvature over the correlation length of the Bragg *patches* is small in some sense. Thus this model replaces the sea surface by an ensemble of *flat* Bragg-scattering patches that are tilted, heaved, and advected by the motion of the large wave components. In its most elementary form, it interprets $\sigma^0(\psi)$ in Eq. (16) as the cross section of a patch with *local* grazing angle $\psi = \psi_0 + \alpha$, where α is the local wave slope and ψ_o is the mean grazing angle. For the simple one-dimensional case, this quantity is averaged over the sea slope distribution $p(\alpha)$, yielding:

$$\bar{\sigma}^0(\psi_0) = \int_{-\infty}^{\infty} \sigma^0(\psi_0 + \alpha)p(\alpha)d\alpha \tag{20}$$

For a more general two-dimensional sea, the local grazing angle is a function of the slopes in and normal to the plane of incidence. For each polarization p, the angle function $F_p(\psi)$ in $\sigma^0(\psi)$ becomes a complex mixture of the angle functions of both polarizations [88]. Reference 90 contains a comprehensive discussion of this model.

Although the composite surface model is often presented as if it emerged as a rigorous product of an integral formulation of the GBVP, it is not a scattering *theory*, but instead is a scattering *picture* assembled from a group of more-or-less plausible assumptions. Such models are never very satisfying, but with the failure of the more formal GBVP theories to provide a general framework for predicting and understanding sea clutter, this model has become the basis for most analytical approaches to backscatter from the sea.

Figure 20 is based on a comparison in Ref. 88 of the predictions of the Bragg model from the SPM (in the form of Eq. (16)) and the composite-surface model (in the form of Eq. (20)) with a sample of NRL 4FR data taken at high wind speeds (>22 kn). The wave spectrum used was the Phillips

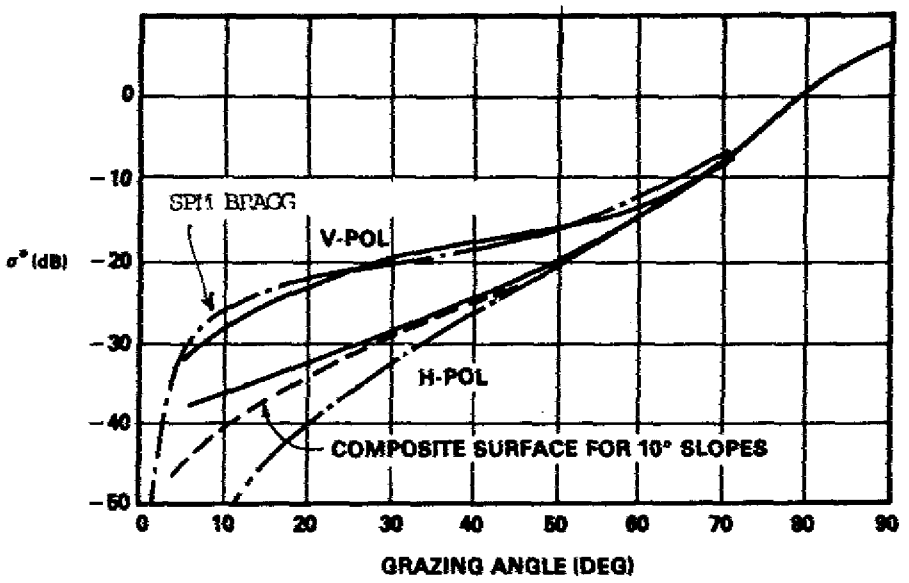

Fig. 20 — Comparison of the predictions of the Bragg hypothesis with NRL-4FR data for higher wind speeds (>20 kn) (based on Valenzuela [88])

spectrum given in Eq. (4). Historically, comparisons of this type have often been used to establish the Bragg scattering hypothesis as a useful clutter model [23, 88, 90], and the agreement usually looks good, especially for the higher wind speeds. But it must be remembered that the small-amplitude approximation in Eq. (16) is by itself totally invalid for the extended sea surface. How a totally invalid application of a scattering approximation can produce results as convincing as those shown for vertical polarization in Fig. 20 remains a curiosity. The effect of using the composite surface model is primarily to introduce an average over surface slopes that raises the horizontal return at the lower grazing angles. However, this effect would also occur if the scattering patch were populated not by Bragg wavelets, but instead by some of the features described in the next section. Nevertheless, agreement between measurement and prediction of the type illustrated in Fig. 20 has sustained belief in the Bragg scattering hypothesis at microwave frequencies despite the lack of a proper theory argued from first principles.

Scattering by Surface Features

The actual sea surface is a complex mixture of wedges, cusps, microbreakers, hydraulic shocks, patches of turbulence, and gravity/capillary waves (both wind-driven and parasitic), punctuated on occasion by the sharp crest of a breaking wave, with plumes of water cascading down its face and a halo of spray above it. In other words, a large variety of scattering features is associated with an active sea surface, any or all of which could contribute to the clutter signal.

The common Stokes wave [83] has a quasi-trochoidal structure that resembles a wedge on the surface, yet only recently were wedges studied as a possible source of sea clutter [11, 12, 74, 75]. The scattering model is usually some variant of the familiar geometrical theory of diffraction (GTD) [91]. This theory is strictly applicable to the clutter problem only when the edge of the wedge is normal to the plane of incidence. Nevertheless, the predictions gave both polarization and grazing angle dependences over at least part of the ranges of these variables that were about as good as, and in some ways better than, the predictions of the Bragg or composite-surface models [75].

One major problem with all models based on scattering features is the lack of any information about the shapes, sizes, orientations, speeds, and lifetimes of the features themselves. For this reason, the predictions of such models must contain arbitrary assumptions about these crucial parameters. However, there is often guidance from either observation or theory. For example, stability arguments prevent the interior angle of a wave crest from falling below 120°, which then becomes a convenient measure of the wedge angle in wedge scattering models. In Fig. 21 the overall scale of wedge scattering as calculated by the GTD was adjusted to place the cluster of cross sections at the level of the experimental values; the polarization and grazing angle dependence is shown by the circles. The dependence on these two parameters appears to be fairly well expressed by the wedge model, although it should be recalled that this model applies only to wedges whose edges are normal to the plane of incidence. The application of GTD-based wedge models confront difficulties just as important as those associated with the application of the Bragg model.

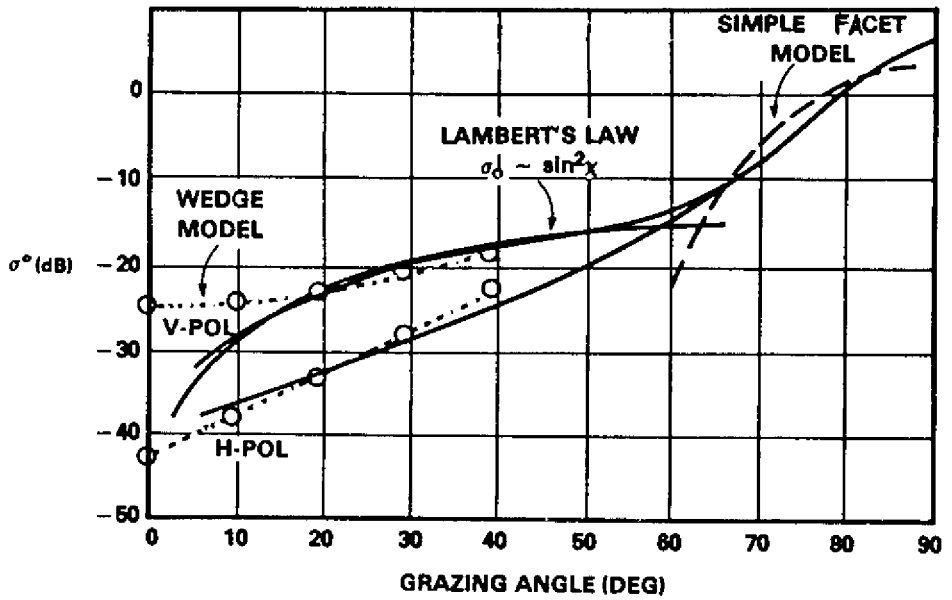

Fig. 21 — Comparison of simple wedge and other models, with NRL-4FR data. (data the same as in Fig. 20).

Figure 21 also compares two very simple scattering models with the data in Fig. 20. Lambert's law, mentioned in connection with Fig. 9, expresses the cross section in the form $\sigma^0 = A \sin^2 \psi$, where A is the surface albedo. Choosing $A = -17$ dB gives a fairly good match to the vertically polarized returns over a wide range of grazing angles. The *facet* model, expressed by Eq. (19) and often thought to describe clutter at the higher grazing angles, is shown for 20 kn seas [88]. The general behavior described by these two models seems to agree about as well as any other, although they too must use arbitrary assumptions to obtain reasonable fits to the data; the significance of this agreement is difficult to assess.

Another surface scattering feature was examined in connection with the complex behavior of sea spikes discovered by Lewis and Olin [33] (see Fig. 11). At low grazing angles, the most visible part of the surface consists of the higher elevations, particularly the peaks and faces of breaking waves. By using a plume model for the scattering elements associated with spilling breakers, a theory of scattering from breaking waves was developed that explained most of the observed behavior of sea spikes [48]. Of course like all other models based on scattering features, arbitrary assumptions had to

be made about the sizes, shapes, and lifetimes of the scattering plumes. But these parameters were all inferred from observation of real sea surfaces, and the resulting predictions were surprisingly good.

Although scattering features have been introduced mainly in connection with low grazing angle sea clutter (Ref. 12 contains a detailed discussion), there is every reason to believe that feature-scattering operates at all grazing angles. Considering the failure of scattering theories formulated as GBVP to provide any predictions beyond those in certain limiting-case approximations and the precarious nature of the logical infrastructure of the Bragg hypothesis in microwave scattering, a careful examination of the actual scattering features present on the sea surface might provide the basis for understanding sea clutter that has been sought for the last 40 years.

SUMMARY AND CONCLUSIONS

In the early days of radar, the importance of knowing the clutter environment led to many experiments under a variety of conditions. Variations in quality and completeness of ground truth, calibration of the equipment, and the competence of the experimenter, led to results that often showed considerable inconsistency and suggested clutter behavior that was sometimes more a function of the vagaries of the experiment than of the physics of clutter. As data of increasingly better quality accumulated, it would seem that the behavior of sea clutter would be established with increasing confidence. This has not always been so. While for the higher 50% of wind speeds encountered over the world's oceans (≥ 15 kn), microwave sea clutter at intermediate-to-high grazing angles has shown little dependence on frequency; the effects of wind speed remain uncertain, seeming to depend on polarization, wind direction, and grazing angle in confusing ways. The major areas of uncertainty, however, lie at any wind speed; whenever the grazing angle goes below a few degrees and the surface illumination begins to feel the effects of refraction and diffraction; and at any grazing angle, whenever the wind speed is ≤ 10 kn, where peculiarities and uncertainties in the generation of surface roughness begin to emerge most strongly.

The jury is still out on the question of sea clutter theory. The most popular model, the composite surface model, is actually an assemblage of assumptions supported by circumstantial evidence; there is still no clear reason why it should work as it does. Theories based on scattering by surface features are beginning to show promise, although the major problem of characterizing these features in a manner useful to quantitative predictions is still to be addressed. It is clear that there is room for considerable work in this fascinating and frustrating field.

REFERENCES

1. M. W. Long, *Radar Reflectivity of Land and Sea* (Artech House, Inc., Dedham, MA, 1983).

2. M. I. Skolnik, *Introduction to Radar Systems* (McGraw-Hill Book Company, New York, 1980).

3. F. E. Nathanson *Radar Design Principles* (McGraw-Hill Book Company, New York, 1983).

4. D. E. Kerr, *Propagation of Short Radio Waves* (McGraw-Hill Book Company, New York, 1951).

5. D. Crombie, "Doppler Spectrum of Sea Echo at 13.56 Mc/s," *Nature* **175**, 681-683 (1955).

6. J. W. Wright, "A New Model for Sea Clutter" *IEEE Trans. Antennas Propag.* **AP-16**, 217-223 (1968).

7. F. G. Bass, I. M. Fuks, A. I. Kalmykov, I. E. Ostruvsky, and A. D. Rosenberg, "Very High Frequency Radio Wave Scattering by a Disturbed Sea Surface," *IEEE Trans. Antenna Propag.* **AP-16**, 554-568 (1968).

8. D. Barrick and Q. Peake, "A Review of Scattering from Surfaces with Different Roughness Scales," *Radio Sci.* **3**, 865-868 (1968).

9. D. Atlas, R. C. Beal, R. A. Brown, P. De Mey, R. K. Moore, C. G. Rapley, and C. T. Swift, "Problems and Future Directions in Remote Sensing of the Oceans and Troposphere: A Workshop Report," *J. Geophys. Res.* **9**(C2), 2525-2548 (1986).

10. D. Holliday, G. St-Cyr and N. E. Woods, "A Radar Ocean Imaging Model for Small to Moderate Incidence Angles," *Int. J. Remote Sensing* **7**, 1809-1834 (1986).

11. D. S. Kwoh, and B. M. Lake, "A Deterministic, Coherent, and Dual-polarized Laboratory Study of Microwave Backscattering from Water Waves, Part 1; Short Gravity Waves without Wind, *IEEE J. Oceanic Eng.* **OE-9**, 291-308 (1984).

12. L. B. Wetzel, "Electromagnetic Scattering from the Sea at Low Grazing Angles," in *Surface Waves and Fluxes: Current Theory and Remote Sensing*, G. L. Geernaert and W. J. Plant, eds., (Reidel, Dordrecht, The Netherlands, 1990), Ch. 12.

13. O. M. Phillips, On Radar Returns from the Sea Surface—Bragg Scattering and Breaking Waves," *IEEE J. Oceanic Eng.*, to be published.

14. D. Middleton, and H. Mellin, "Wind-Generated Solitons: A Potentially Significant Mechanism in Ocean Surface Wave Generation and Wave Scattering," *IEEE J. Oceanic Eng.*, **OE-10**, 471-476, (1985).

15. S. Tang and O. H. Shemdin, "Measurement of High-frequency Waves using a Wave Follower," *J. Geophys. Res.* **88**, 9832-9840 (1983).

16. W. J. Pierson and L. Moskowitz, "A Proposed Spectral Form for Fully Developed Seas based on the Similarity Theory of S. A. Kitaigorodskii," *J. Geophys. Res.*, **69**, 5181-5190, (1964).

17. O. M. Phillips, *The Dynamics of the Upper Ocean,* 2nd ed. (Cambridge University Press, Cambridge, 1977).

18. W. J. Pierson, Jr. and M. A. Donelan, "Radar Scattering and Equilibrium Ranges in Wind-Generated Waves with Application to Scatterometry," *J. Geophys. Res.* **91**(C5), 4971-5029 (1987).

19. S. A. Kitaigorodskii, "On the Theory of the Equilibrium Range in the Spectrum of Wind-Generated Gravity Waves," *J. Phys. Oceanogr.* **13**, 816-827, (1983).

20. O. M. Phillips, "Spectral and Statistical Properties of the Equilibrium Range in Wind-Generated Gravity Waves," *J. Fluid Mech.* **156**, 505-531 (1985).

21. J. C. Daley, J. T. Ransone, J. A. Burkett, and J. R. Duncan, "Sea Clutter Measurements on Four Frequencies," NRL Report 6806, Nov. 1968.

22. G. R. Valenzuela and R. Laing: On the Statistics of Sea Clutter, NRL Report 7349, Dec. 1971.

23. N. W. Guinard, J. T. Ransone, Jr., and J. C. Daley, "Variation of the NRCS of the Sea with Increasing Roughness," *J. Geophys. Res.* **76**, 1525-1538 (1971).

24. J. C. Daley, "Wind Dependence of Radar Sea Return," *J. Geophys. Res.* **78**, 7823-7833 (1973).

25. A. I. Kalmykov and V. V. Pustovoytenko "On Polarization Features of Radio Signals Scattered from the Sea Surface at Small Grazing Angles," *J. Geophys. Res.*, **81**, 1960-1964 (1976).

26. I. Katz, and L. M. Spetner, "Polarization and Depression Angle Dependence of Radar Terrain Return," *J. Res. NBS-D* **64-D**, 483-486 (1960).

27. F. Feindt, V. Wismann, W. Alpers, and W. C. Keller "Airborne Measurements of the Ocean Radar Cross Section at 5.3 GHz as a Function of Wind Speed," *Radio Sci.* **21**, 845-856 (1986).

28. L. C. Schroeder, P. R. Schaffner, J. L. Mitchell, and W. L. Jones, "AAFE RADSCAT 13.9-GHz Measurements and Analysis: Wind-Speed Signature of the Ocean," *IEEE J. Oceanic Eng.* **OE-10**, 346-357 (1985).

29. H. Masuko, K. Okamoto, M. Shimada, and S. Niwa, "Measurement of Microwave Backscattering Signatures of the Ocean Surface Using X Band and Ka Band Airborne Scatterometers," *J. Geophys. Res.*, **91**(C11), 13065-13083 (1986).

30. A. H. Chaudhry and R. K. Moore, "Tower-Based Backscatter Measurements of the Sea," *IEEE J. Oceanic Eng.* **OE-9**, 309-316, (1984).

31. G. P. de Loor and P. Hoogeboom, "Radar Backscatter Measurements from Platform Noordwijk in the North Sea," *IEEE J. Oceanic Eng.* **OE-7**, 15-20 (1982).

32. F. T. Ulaby, R. K. Moore, and A. K. Fung; *Microwave Remote Sensing, Active and Passive: Vol. III*, (Addison-Wesley Publishing Company, Reading, Mass., 1986), Section 20.2.

33. B. L. Lewis, and I. D. Olin, "Experimental Study and Theoretical Model of High-Resolution Backscatter from the Sea," *Radio Sci.* **15**, 815-826 (1980).

34. D. Trizna, "Measurement and Interpretation of North Atlantic Ocean Marine Radar Sea Scatter," NRL Report 9099, May, 1988.

35. G. V. Trunk, "Radar Properties of Non-Rayleigh Sea Clutter," *IEEE Trans. Aerospace Electron. Syst.* **8**(2), 196-204 (1972).

36. Jin Wu, "Variations of Whitecap Coverage with Wind Stress and Water Temperature," *J. Phys. Oceanogr.* **18(10)** 1448-1453 (1988).

37. M. Katzin, "On the Mechanisms of Radar Sea Clutter," *Proc. IRE* **45**, 44-54 (1957).

38. L. B. Wetzel, "A Model for Sea Backscatter Intermittency at Extreme Grazing Angles," *Radio Sci.* 12, 749-756 (1977).

39. I. M. Hunter and T. B. A. Senior, "Experimental Studies of Sea Surface Effects on Low Angle Radars," *Proc. IEE*, **113**, 1731-1740 (1966).

40. H. Sittrop, "X- and Ku-Band Radar Backscatter Characteristics of Sea Clutter," *Proc. of the URSI Commission II Specialist Meeting on Microwave Scattering from the Earth,* E. Schanda, ed., Berne, Switzerland, 1974.

41. B. "G. Smith, Geometrical Shadowing of the Random Rough Surface," *IEEE Trans. Antennas Propag.* **AP-15**, 668-671 (1967).

42. F. B. Dyer and N. C. Currie, "Some Comments on the Characterization of Radar Sea Echo," Digest of the International IEEE Symposium on Antennas and Propagation, July 10-12, 1974.

43. D. E. Barrick, J. M. Headrick, R. W. Bogle, and D. D. Crombie, "Sea Backscatter at HF: Interpretation and Utilization of the Echo, *Proc. IEEE*, **62**(6), (1974).

44. C. C. Teague, G. L. Tyler, and R. H. Stewart, "Studies of the Sea Using HF Radio Scatter," *IEEE J. Oceanic Eng.* **OE-2**, 12-19 (1977).

45. J. C. Wiltse, S. P. Schlesinger, and C. M. Johnson, "Back-Scattering Characteristics of the Sea in the Region from 10 to 50 KMC," *Proc. IRE*, **45**, 220-228 (1957).

46. G. W. Ewell, M. M. Horst, and M. T. Tuley, "Predicting the Performance of Low-angle Microwave Search Radars—Targets, Sea Clutter, and the Detection Process," Proceedings of OCEANS 79, pp. 373-378, 1979.

47. W. K. Rivers, "Low-angle Radar Sea Return at 3-mm Wavelength," Engineering Experiment Station, Georgia Institute of Technology, Final Technical Report, Contract N62269-70-C-0489, November, 1970.

48. L. B. Wetzel, "On Microwave Scattering by Breaking Waves," Chapter 18 in *Wave Dynamics and Radio Probing of the Ocean Surface*, O. M. Phillips and K. Hasselmann, eds. (Plenum Press, New York, 1986) pp. 273-284.

49. B. L. Hicks, N. Knable, J. J. Kovaly, G. S. Newell, J. P. Ruina, and C. W. Sherwin, "The Spectrum of X-Band Radiation Backscattered from the Sea Surface," *J. Geophys. Res.* **65**, 825-837, (1960).

50. G. R. Valenzuela, and R. Laing, "Study of Doppler Spectra of Radar Sea Echo," *J. Geophys. Res.* **65**, 551-562 (1970).

51. V. W. Pidgeon, "Doppler Dependence of Sea Return." *J. Geophys. Res.* **73**, 1333-1341 (1968).

52. Y. U. Mel'nichuk, and A. A. Chernikov, "Spectra of Radar Signals from Sea Surface for Different Polarizations," *Izvestia, Atmos. Oceanic. Phys.* **7**, 28-40 (1971).

53. J. W. Wright and W. C. Keller, "Doppler Spectra in Microwave Scattering from Wind Waves," *Phys. Fluids* **14**, 466-474 (1971).

54. D. Trizna, "A Model for Doppler Peak Spectral Shift for Low Grazing Angle Sea Scatter," *IEEE J. Oceanic Eng.* **OE-10**, 368-375 (1985).

55. W. C. Keller, W. J. Plant, and G. R. Valenzuela, "Observation of Breaking Ocean Waves with Coherent Microwave Radar," in *Wave Dynamics and Radio Probing of the Ocean Surface*, O. M. Phillips and K. Hasselmann, eds., (Plenum Press, New York, 1986). Ch. 19, pp. 285-292.

56. R. K. Moore, Y. S. Yu, A. K. Fung, D. Kaneko, G. J. Dome, and R. E. Werp, "Preliminary Study of Rain Effects on Radar Scattering from Water Surfaces," *IEEE J. Oceanic Eng.* **OE-4**, 31-32 (1979).

57. J. P. Hansen, "High Resolution Radar Backscatter from a Rain Disturbed Sea Surface," ISNR-84 Record, October 22-24, Tokyo, Japan, 1984.

58. J. P. Hansen, "A System for Performing Ultra High Resolution Backscatter Measurements of Splashes," Proceedings of the International Microwave Theory and Techniques Symposium, Baltimore, Maryland, 1986.

59. L. B. Wetzel, "On the Theory of Electromagnetic Scattering from a Raindrop Splash" NRL Memorandum Report 6103, Dec. 1987.

60. L. B. Wetzel, "On the Origin of Long-Period Features in Low-Angle Sea Backscatter," *Radio Sci.* **13**, 313-320 (1978).

61. W. Garrett, "Physicochemical Effects of Organic Films at the Sea Surface and their Role in the Interpretation of Remotely Sensed Imagery," ONRL Workshop Proceedings Role of Surfactant Films on the Interfacial Properties of the Sea Surface, F. L. Herr and J. Williams, eds. pp. 1-18, November 21, 1986.

62. H. Huhnerfuss, W. Alpers, W. D. Garrett, P. A. Lange, and S. Stolte, "Attenuation of Capillary and Gravity Waves at Sea by Monomolecular Organic Surface Films," *J. Geophys. Res.* **88**, 9809-9816 (1983).

63. J. C. Scott, "Surface Films in Oceanography," ONRL Workshop Proceedings - *Role of Surfactant Films on the Interfacial Properties of the Sea Surface*, F. L. Herr and J. Williams, eds. 19-40, November 21, 1986.

64. N. W. Guinard, "Radar Detection of Oil Spills, "Joint Conference on Sensing of Environmental Pollutants, Palo Alto, California, AIAA Paper No.71-1072, November 8-10, 1971.

65. H. Huhnerfuss, W. Alpers, A. Cross, W. D. Garrett, W. C. Keller, P. A. Lange, W. J. Plant, F. Schlude, and D. L. Schuler, *"The Modification of X and L Band Radar Signals by Monomolecular Sea Slicks," J. Geophys. Res.* **88**, 9817-9822 (1983).

66. C. S. Cox, and W. H. Munk, "Statistics of the Sea Surface Derived from Sun Glitter," *J. Mar. Res.* **13**, 198-227 (1954).

67. R. B. Perry, and G. R. Schimke, "Large-Amplitude Internal Waves Observed off the Northwest Coast of Sumatra," *J. Geophys. Res.* **70**, 2319-2324, (1965).

68. W. Alpers, and I. Hennings, "A Theory of the Imaging Mechanism of Underwater Bottom Topography by Real and Synthetic Aperture Radar," *J. Geophys. Res.* **89**, 10529-10546 (1984).

69. D. Trizna, private communication.

70. H. Goldstein, "Frequency Dependence of the Properties of Sea Echo," *Phys. Rev.* **70**, 938-946, (1946).

71. A. H. "Schooley, Some Limiting Cases of Radar Sea Clutter Noise," *Proc. I.R.E.* **44**, 1043-1047 (1956).

72. W. S. Ament, "Forward and Backscattering by Certain Rough Surfaces," *Trans. I.R.E* **AP-4, 369-373 (1956).**

73. V. Twersky,"On the Scattering and Reflection of Electromagnetic Waves by Rough Surfaces, *Trans. I.R.E.* **AP-5**, 81-90 (1957).

74. D. R. Lyzenga, A. L. Maffett, and R. A. Schuchman, "The Contribution of Wedge Scattering to the Radar Cross Section of the Ocean Surface," *IEEE Trans. Geosci. Remote Sensing,* **GE-21**, 502-505, (1983).

75. L. B. Wetzel, "A Minimalist Approach to Sea Backscatter - the Wedge Model," URSI Open Symposium on Wave Propagation: Remote Sensing and Communication, Univ. of New Hampshire, Durham, N. H., Preprint Volume pp. 3.1.1-3.1.4, July 28-August 1, 1986.

76. S. O. Rice, "Reflection of Electromagnetic Waves from Slightly Rough Surfaces, *Commun. Pure Appl. Math.* **4**, 361-378 (1951).

77. W. H. Peake, "Theory of Radar Return from Terrain," IRE National Convention Record Vol. 7, pp. 27-41, 1959.

78. G. R. Valenzuela, "Depolarization of EM Waves by Slightly Rough Surfaces," *IEEE Trans. Antennas Propag.* **AP-15**, 552-559 (1967).

79. F. G. Bass, and I. M. Fuks, *Wave Scattering from Statistically Rough Surfaces* (Pergamon Press, New York, 1979).

80. C. Eckart, "The Scattering of Sound from the Sea Surface," *J. Acoust. Soc. Am.* **25**, 566-570 (1953).

81. P. Beckmann, and A. Spizzichino, *The Scattering of Electromagnetic Waves from Rough Surfaces* (Macmillan, New York, 1963).

82. L. B. Wetzel, "HF Sea Scatter and Ocean Wave Spectra," URSI Spring Meeting, National Academy of Sciences, Washington, D.C., April, 1966.

83. B. Kinsman, *Wind Waves* (Prentice-Hall, Englewood Cliffs, N. J., 1965).

84. A. K. Fung, and G. W. Pan, "A Scattering Model for Perfectly Conducting Random Surfaces: I. Model Development," *Int. J. Remote Sensing* **8**(11), 1579-1593 (1987).

85. F. B. Dyer, and N. C. Currie, "Some Comments on the Characterization of Radar Sea Echo," Digest of the International IEEE Symposium on Antennas and Propagation, pp. 323-326, June 10-12, 1974.

86. D. E. Barrick, "Extraction of Wave Parameters from Measured HF Sea Echo Doppler Spectra," *Radio Sci.* **12**, 415-424 (1977).

87. J. W. Maresca, and T. M. Georges, "Measuring RMS Wave Height and the Scalar Ocean Wave Spectrum with HF Skywave Radar," *J. Geophys. Res.* **85**, 2759-2771 (1980).

88. G. R. Valenzuela, "Theories for the Interaction of Electromagnetic and Oceanic Waves - A Review," *Boundary-Layer Meteorology*, **13**, 61-85 (1978).

89. B. F. Kuryanov, "The Scattering of Sound at a Rough Surface with Two Types of Irregularity," *Sov. Phys. Acoust.* **8**, 252-257 (1963).

90. W. J. Plant, "Bragg Scattering of Electromagnetic Waves from the Air/Sea Interface," in *Surface Waves and Fluxes: Current Theory and Remote Sensing* G. L. Geernaert and W. J. Plant, eds., (Reidel, Dordrecht, The Netherlands, 1990) Ch. 12.

91. J. B. Keller, "Diffraction by an Aperture," *J. Appl. Phys.* **28**, 426-444 (1957).

92. W. Alpers and H. Huhnerfuss, "Radar Signatures of Oil Films Floating on the Sea Surface and the Marangoni Effect," *J. Geophys. Res.* **93**(C4), 3642-3648 (1988).

93. H. Masuko, and H. Inomata, "Observations of Artificial Slicks by X and Ka Band Airborne Scatterometers," Proceedings of the 1988 International Geoscience and Remote Sensing Symposium (IGARSS'88), Edinburgh, UK, 12-16 September, 1988, pp. 1089-1090, Published by the European Space Agency, ESTEC, Noordwijk, The Netherlands, 1988.